Nanoscale Research Letters

REVIEW Open Access

Silver Halide-Based Nanomaterials in Biomedical Applications and Biosensing Diagnostics

Lin Zhang and Hong Zhang*

Abstract

In recent years, silver halide (AgX, X = Cl, Br, I)-based photocatalytic materials have received increasing research attention owing to their excellent visible-light-driven photocatalytic performance for applications in organic pollutant degradation, HER, OER, and biomedical engineering. Ag as a noble metal has a surface plasma effect and can form Schottky junctions with AgX, which significantly promotes electron transport and increases photocatalytic efficiency. Therefore, Ag/AgX can reduce the recombination rate of electrons and holes more than pure AgX, leading to using AgX as a photocatalytic material in biomedical applications. The use of AgX-based materials in photocatalytic fields can be classified into three categories: AgX (Ag/AgX), AgX composites, and supported AgX materials. In this review, we introduce recent developments made in biomedical applications and biosensing diagnostics of AgX (Ag/AgX) photocatalytic materials. In addition, this review also discusses the photocatalytic mechanism and applications of AgX (Ag/AgX) and supported AgX materials.

Keywords: AgX nanomaterials, Photodynamic therapy, Antibacterial, Biosensors

Introduction

Among various types of inorganic nanoparticles (NPs), silver NPs (AgNPs), due to their unique chemical, physical, and biological properties, have received a lot of attention for biomedical and bioanalytical applications [1–5]. For example, AgNPs are well known for their highly effective antimicrobial activities [2, 4, 6, 7] both in solutions and in solids. In addition, AgNPs have been widely used in several areas, such as sterilization [8–10], iconography, [11–13] water treatment [14–16], food package [17–19], agriculture [20–23], medicine [24–27], photocatalysis [28, 29], biotechnology [30–32], cancer therapy [33–37], Raman spectroscopy [38–40], electrochemistry [41–44], and environmental monitoring [44–47].

AgNPs can be combined with other nanomaterials to improve their performance. For example, AgNPs can be reduced on some semiconductors (such as TiO_2, ZnO, and WO_3) to form the Schottky junction [33, 48–50]. AgNPs have also been combined with magnetic NPs [51], graphene oxide [52], and quantum dots for various applications [53].

Silver halides have been widely used as industrial catalysts and photosensitive materials [54–61], and the use of silver halides is discussed in the following part. Chemically, silver has a strong affinity with halides to form various AgX (X = Cl, Br, and I) materials. There are numerous methods to prepare Ag/AgX. For example, AgX is doped on the surface of AgNPs by exposure to light of appropriate wavelengths, high-temperature reduction, and reducing agents. Ag/AgX shows better activity and selectivity toward certain applications. Thus, Ag/AgX as a nanocomposite has been extensively researched in recent years [8, 54, 62–68].

Since silver chloride has very low solubility in water, it is often used in the laboratory to determine the silver content of samples. Another very important application

*Correspondence: zhanghong_szy@163.com

Shandong University of Traditional Chinese Medicine Affiliated Hospital, No. 16369, Jingshi Road, Jinan 250014, Shandong, People's Republic of China

of silver chloride in electrochemistry is to make silver/silver chloride reference electrodes [69]. AgBr has been applied in several areas [70], such as color-changing lenses, in which a very small amount of silver bromide and copper oxide were added to ordinary glass. AgBr has photosensitivity and is often used in photographic films. A thin layer of gelatin containing fine AgBr NPs is coated on printing paper. When light with different intensities hit the film, AgBr decomposition products of different degrees are produced on the film. The more AgBr breaks down, the more darkness on that part. At last, AgI can condense water vapor in the air and form rain. Thus, AgI has been used as a nucleating reagent to precipitate supercold clouds and induce artificial rain. Aside from the above traditional applications, the photosensitivity of AgX has been recently utilized in biomedical and bioanalytical applications [71–73].

Although AgX can be applied in numerous ways, there are still some challenges and limitations. For example, AgX responds to ultraviolet and visible light, but light in this wavelength range cannot penetrate most human tissues. When applied to clinical studies, the toxicity of AgX has not been thoroughly studied. In some photocatalytic systems, photocorrosion of AgX can occur. Over the last few decades, a large surge in research activities emerged for biological applications of nanomaterials. Among them, the use of AgX has been growing most rapidly. Most related works were published in the last 15 years. In this article, we review the current status of the field with a focus on anticancer, antibacterial applications, and bioanalytical sensors.

Photocatalytic Activities of AgX

Before reviewing examples of various applications, we first describe the mechanism of photocatalytic activities, which are the basis for the design of materials and their properties. The principle of photocatalysis is based on the redox activity of photocatalysts under light to achieve degrading pollutants, material synthesis, and chemical transformations. Normally, photocatalytic oxidation uses semiconductors as catalysts and light as energy to degrade organic matter into carbon dioxide and water, where advanced oxidation by TiO_2 is a primary example [48, 56, 74–76].

AgX belongs to semiconductors, and the bandgaps of AgCl, AgBr, and AgI are 3.28, 2.89, and 2.22 eV, respectively [77]. Pure AgX as a semiconductor has a low photocatalytic efficiency under ambient light irradiation [78–80]. Nevertheless, Ag nano-dots can still swiftly grow on the surface of AgX even with weak light irradiation [8, 54, 65–67, 69], which generates Ag/AgX nanocomposites.

The photocatalytic mechanism of Ag/AgX nanocomposites is displayed in Fig. 1. The Ag metal as a conductor grown on the surface of AgX can easily generate electron–hole pairs, and then those electrons in the valance band can absorb the photons with energy equal to or higher than the bandgap energy. Those photo-generated charge carriers can only be deactivated by O_2 or H_2O. The first process is the photo-generated charge-mediate redox reactions, which include the oxidation of H_2O to form $OH^{\cdot}$ radicals, and the reduction of O_2 to form reactive oxygen species (e.g., singlet oxygen, hydroxyl radical, superoxide, hydroperoxyl radical, and hydrogen peroxide) [81, 82]. This is the main process that can generate ROS. The second process is deactivation, which produces electron–hole pairs on the other side and recombines to obstruct redox reactions. Therefore, the second process decreases the efficiency of photocatalysis, which explains why pure AgNPs have a weak photocatalysis activity.

To inhibit the second process, that photo-generated charge recombination can be decreased by adding a semiconductor photocatalyst, such as AgX. AgX coated on AgNPs would naturally form a Schottky junction, which is supposed to trap the photo-generated charge carriers and then provide free electrons to minimize the recombination process [83–87]. Those electron–hole pairs generated by photo-excitation would migrate from AgNPs to the conduction band of AgX. In other words, these excess electrons in the semiconductor (AgX) side will migrate to holes in the metal side (Ag) through the Schottky junction.

Meanwhile, a large number of electrons generated by AgNPs can accelerate the process of photocatalysis, because of the localized surface plasmon resonance (LSPR) of AgNPs [57–59, 88–90]. Noble metal NPs, such as Au, Ag, Pt, and Cu, exhibit strong UV–Vis absorption due to their surface plasmon resonance (SPR). When AgX is decomposed into Ag^0, the nanocomposite can demonstrate strong SPR and enhance the photocatalytic ability. As a result, plasmonic NPs can serve as an alternative type of sensitizer to enhance the visible light absorption of photocatalysts without the problem of degradation like organic sensitizers [91–93]. In 2008, Wang et al. fabricated Ag/AgCl plasmonic photocatalysts by an ion-exchange method [58], which triggered an upsurge in researching Ag/AgX plasmonic photocatalysts.

AgX for Cancer Therapy

Cancer has the biological characteristics of abnormal cell differentiation and proliferation, loss of control of growth, invasion, and metastasis. In 2020, an estimated 19.3 million new cancer cases and almost 10.0 million cancer deaths occurred worldwide. The most common cancers are esophagus, lung, stomach, breast, and

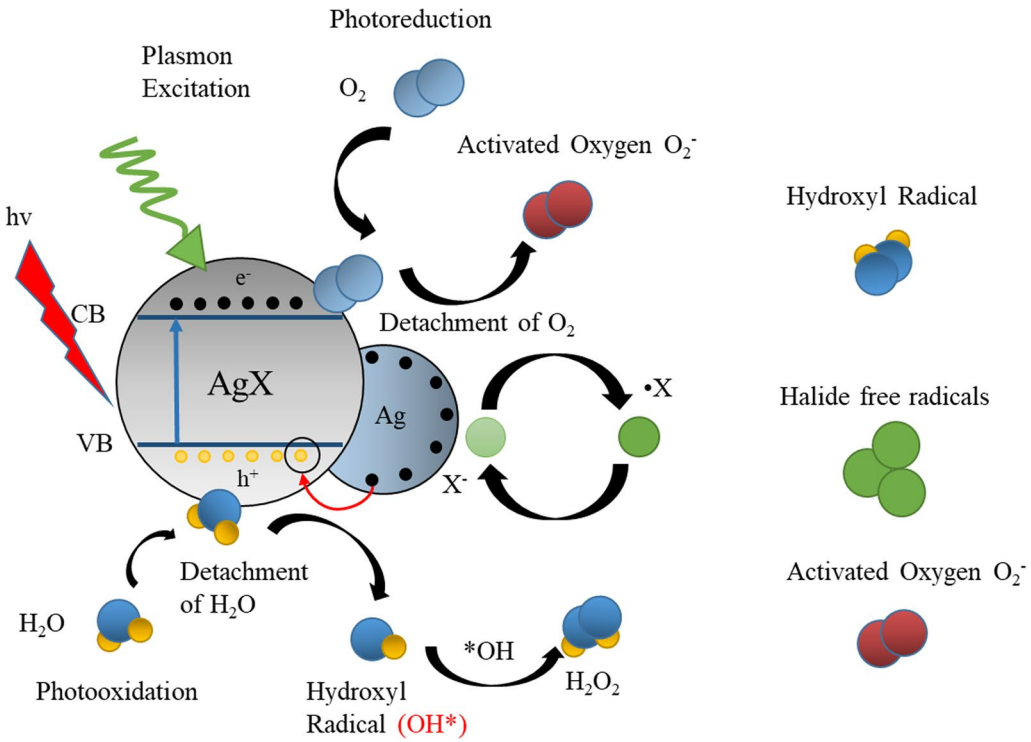

Fig. 1 The photocatalytic mechanism of AgX and AgNPs. The AgX as a semiconductor absorbs photons under light irradiation, which generates photoelectron–hole pairs when the energy is greater than the bandgap. The photocarriers migrate to the surface under the action of the electric field or by diffusion motion. The electrons and holes migrate to the surface of the catalyst and react with the adsorbed material on the surface of the catalyst, respectively. Meanwhile, Ag as a conductor can promote electron transfer to the holes on AgX NPs

cervical cancers. According to the analysis, the global cancer burden would increase by 28.4 million cases in 2040, a 47% rise from 2020. Meanwhile, a larger increase in developing (64% to 95%) countries will occur than in developed (32% to 56%) countries [94]. Therefore, nanotechnology in cancer treatment and diagnosis has gained popularity because it may have fewer side effects than traditional chemotherapeutics, and radiation therapy, which can generate cytotoxicity to normal cells as well [95–101]. To enhance the therapeutic effect and decreases the side effects, photodynamic therapy (PDT) is widely used in cancer treatment today [102–110].

AgX-based nanostructures have high biocompatibility, photocatalytic ability, and low toxicity, which have been regarded as attractive candidates to increase the clinical therapeutic effect of numerous kinds of cancer such as skin cancer and mouth cancer [33, 68, 96, 111]. Due to the limitation of effective wavelength, most current organic photosensitizers (less than 600 nm) cannot be used for tissues thicker than 0.1 cm since light cannot reach them. In addition, these organic photosensitizers are sometimes difficult to be excreted from the body. The wavelength range of AgX photosensitizers can be adjusted, and the application of a far infrared band can produce photothermal and photodynamic combined therapy. Since the particles can become smaller, they can be metabolized by the human body. In the following section, we review representative studies of Ag/AgX nanostructures in targeted drug delivery and controlled release systems.

Photodynamic Therapy

In PDT, the tumor site is irradiated under the light of specific wavelengths to activate photosensitive drugs, selectively concentrate them in the tumor tissue, and trigger photochemical reactions to destroy the tumor. The superoxide disproportionation reaction occurs under light irradiation. Photosensitive drugs can generate ROS (hydroxyl free radicals and superoxide free radicals), which can produce cytotoxicity and kill tumor cells. PDT has the advantage of delivering precise and effective treatments with fewer side effects than traditional cancer therapies.

Wang et al. reported DNA-templated plasmonic Ag/AgCl nanostructures in 2013 [111], which have selective photocatalysis and photocatalytic ability for killing cancer cells. They introduced DNA-programmable synthesis of ~20 nm Ag/AgCl nanostructures by short-term

(5 min) UV irradiation as shown in Fig. 2A, yielding monodispersed AgNPs in the presence of DNA. Moreover, these optimal DNA-encapsulated structures show DNA sequence-specific sizes down to less than 40 nm with an Ag/AgCl composition ratio of 2: 1 that afforded a vastly increased surface area and higher photocatalytic activity. The cell counting kit-8 (CCK-8) cytotoxicity assay showed a decrease of around 75% in the viability of the photocatalyst-treated HeLa cells with 532 nm light irradiation for 8 min (Fig. 2B).

In 2011, Seo's group reported that serum protein-adsorbed Ag/AgBr/TiO_2 NPs have photocytotoxicity in vitro and in vivo under visible light [112]. In this case, both Ag/AgBr and TiO_2 had photocatalytic activities. The authors prepared Ag/AgBr/TiO_2 by the deposition–precipitation method and found that they appeared to be well internalized by human carcinoma cells. As shown in Fig. 3A, the authors tested two types of cancer cells including human cervical HeLa and skin A431 cancer cells after incubation with and without the Ag/AgBr/TiO_2 and subsequent exposure to visible light from a halogen lamp. Fluorescence images were taken to evaluate the labeled mitochondria activity, and the results suggested that ROS triggered the photo-destruction of the cancer cells. After applying the halogen light illumination for 50–250 min and ~8 ppm (μg/mL) of the photocatalytic Ag/AgBr/TiO_2, the authors observed a 40–60% decrease in cell viability (Fig. 3B). Finally, the Ag/AgBr/TiO_2 was

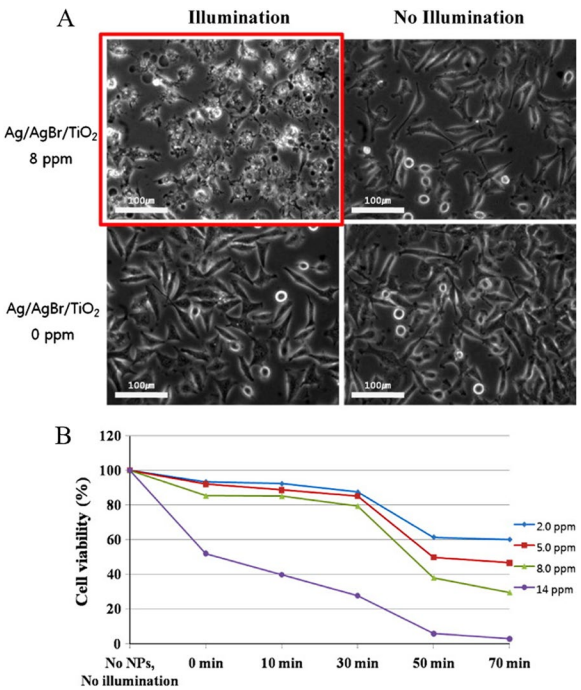

Fig. 3 **A** Optical inverted phase-contrast microscopy images for the viability of HeLa cells treated with Ag/AgBr/TiO_2 NPs incubated for longer than 24 h. Viability of HeLa cells as a function of halogen light illumination time. **B** The trypan blue exclusion test. The cells were treated with different Ag/AgBr/TiO_2 NPs concentrations in the range of 2.0, 5.0, 8.0, and 14.0 ppm. Adapted from Ref. [112] with permission. Copyright (2011), Journal of Hazardous Materials

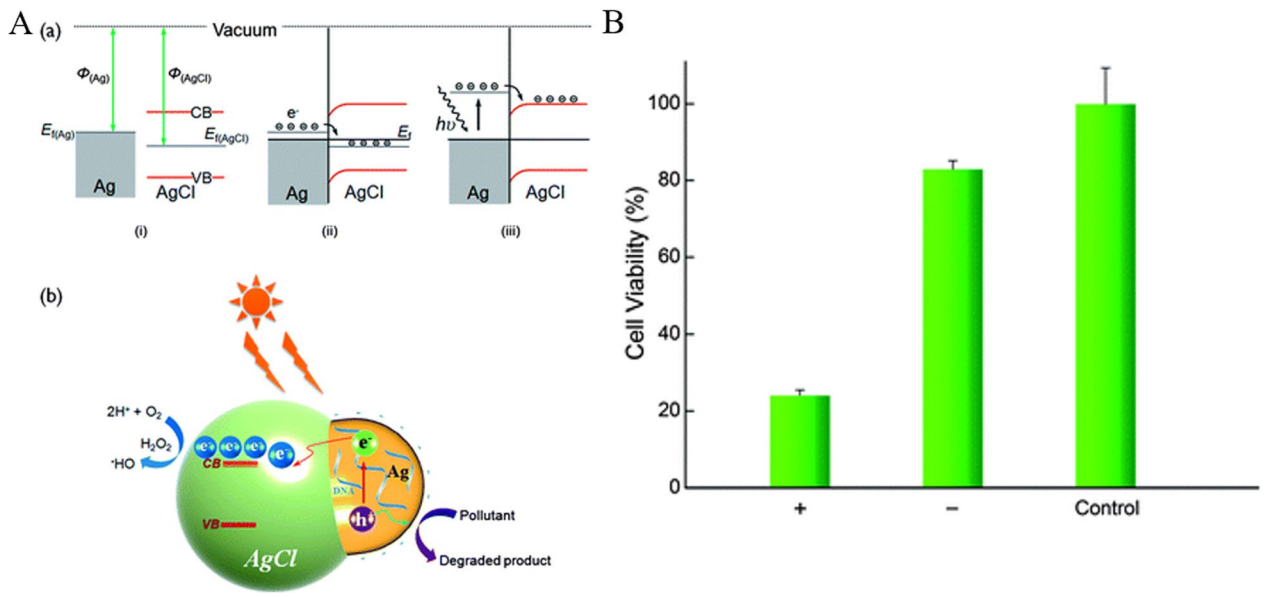

Fig. 2 **A** Illustration of the plasmonic Ag/AgCl nanostructure-based photocatalytic reaction mechanism. The DNA capping makes silver nanostructures negatively charged. **B** A comparison of viability among HeLa cells incubated with (+) and without (−) the Ag/AgCl nanostructures in PBS after photo-irradiation for 8 min. Adapted from Ref. [111] with permission. Copyright (2013), Journal of Materials Chemistry B

found to eliminate xenograft tumors significantly by irradiating visible light in vivo for 10 min.

The above two examples had either DNA or TiO_2 on the surface of Ag/AgX. In 2021, Zhang et al. reported that naked Ag/AgCl NPs can be applied for photocatalytic cancer treatment [68]. In this work, the authors synthesized biocompatible and surfactant-free Ag/AgCl NPs to investigate the photocatalytic efficacy. AgCl can be oxidized by $FeCl_3$ on the surface of AgNPs, which naturally formed a Schottky junction. Thus, Ag as a co-catalyst can easily trap the photo-generated charge carriers and then provide free electrons, which would decrease the influence of the recombination process and increase photocatalytic efficacy. The photocatalytic efficacy of the Ag/AgCl NPs eliminated over 75% of HeLa cells under 30 min of light irradiation (Fig. 4A). Besides that, light irradiation stimulated the SPR of the AgNPs, which can enhance visible light absorption by the material. Compared to the pure AgNPs, the AgCl-coated AgNPs had a broader range of working wavelengths and higher photocatalytic efficacy (Fig. 4B). Moreover, it has less dark cytotoxicity than the pure AgCl NPs.

Cancer Cell Detection

An early cancer diagnosis is critical for the treatment and survival of cancer patients. Its purpose is to detect and treat early, and to reduce the physical, mental and economic burden of patients. Early cancer physical examination methods include a series of new cancer physical examination methods such as blood drop detection, genetic testing, nano-detection, and imaging [113, 114]. Laboratory tests can be used to analyze tumor markers, which substances are higher than normal levels found in the blood, urine, or tissues of some cancer patients. Imaging tests used to diagnose cancer may include computed tomography (CT) scans, bone scans, magnetic resonance imaging (MRI), positron emission tomography (PET) scans, ultrasound, and X-rays.

The methods for cancer cell detection can be conducted in two simple approaches. The first is that Ag/AgX nanomaterials can be composited with specific aptamers for cancer cells or folic acid (FA). Then, tumor-specific antigens or folate receptors will attract and bind the nanomaterials on those tumor cells. After that, colorless TMB is added in vitro and in vivo, which can be oxidized by Ag/AgX nanomaterials under light irradiation to blue-colored oxTMB, which can stain the tumor area. The second approach takes advantage of a high level of glutathione (GHS) in the tumor microenvironment, which has been generally regarded as a characteristic of cancerous tissues. AgBr nanomaterials can react with glutathione (GHS) to form AgNPs, which have a strong photoacoustic (PA) signal in the NIR-II region.

Silver halide has excellent imaging capability based on its physical property, which can be used in cancer detection. In 2014, Wang et al. reported a series of chitosan (CS) modified AgX NPs, which had dual-responsive enzyme mimetic activities [115]. In the presence of H_2O_2, the CS/AgX NPs were able to oxidize various colorimetric dyes, namely, peroxidase-like activity. Upon photoactivation, CS-AgX NPs could also oxidize the typical substrates in the absence of H_2O_2. Thus, the CS-modified silver halide was found to have dual-responsive enzyme mimetic activities. Based on these findings, the CS-AgI was regarded as a cost-effective, rapid, and highly sensitive colorimetric assay to detect cancer cells under light irradiation. The detection limit of the method for MDA-MB-231 was estimated to be as low as 100 cells, which

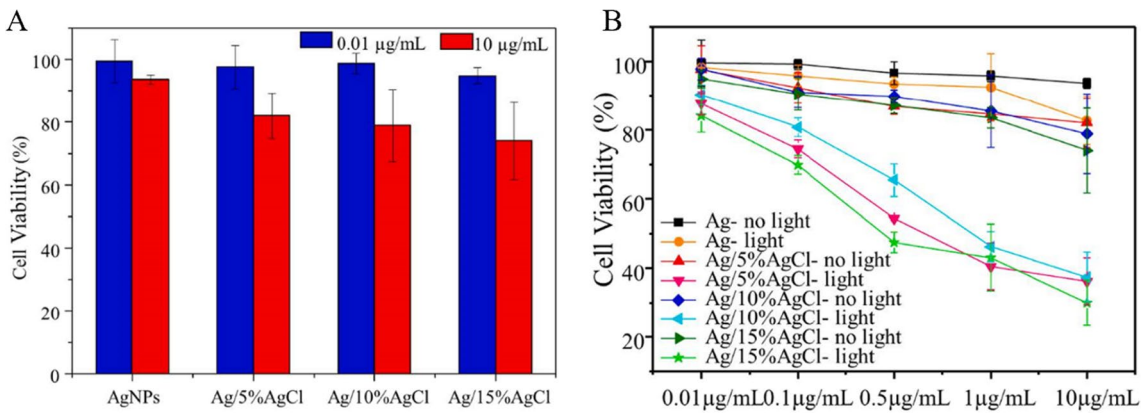

Fig. 4 **A** The cell viability of Ag and different ratios of AgCl at Ag treated HeLa cells in a dark environment. **B** The comparison of HeLa cell viability treated by Ag and Ag/AgCl with or without simulated sunlight. Adapted from Ref. [68] with permission. Copyright (2022), Chemical Engineering Journal

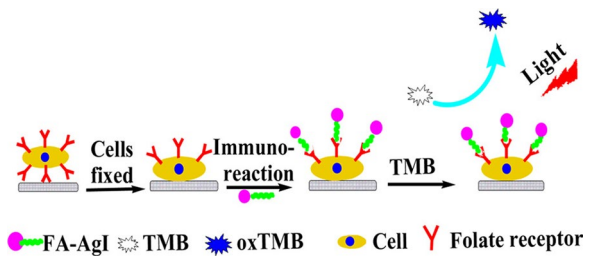

Fig. 5 Proposed detection process using FA-CS-AgI. Adapted from Ref. [115] with permission. Copyright (2014) ACS Publications

was much lower than that reported by the method using peroxidase mimicking nanozymes based on other nanomaterials [116, 117].

Folic acid (FA), one of the best-characterized biological ligands, is widely employed to target tumors or cancer cells because folate receptors are usually overexpressed on the membrane of human cancer cells [118, 119]. FA-CS-AgI conjugates were synthesized by chemically coupling FA to CS via the formation of an amide bond between the amine groups of CS and the carboxyl groups of FA. As Fig. 5 shows, cells were first fixed on a

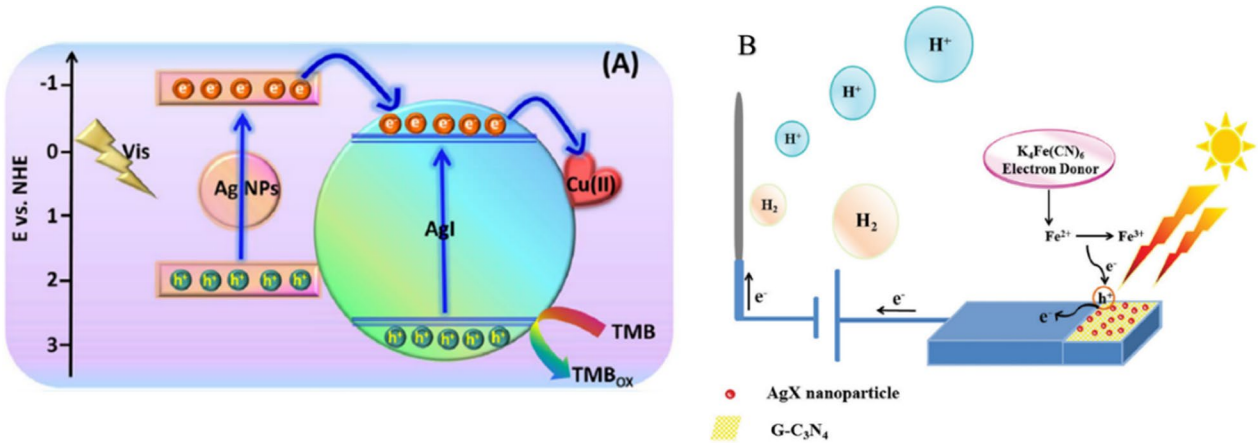

Fig. 6 **A** The schematic illustration of oxidation of TMB by Cu^{2+}/Ag–AgI **B** Photo-generated electron–hole transfer mechanism of C_3N_4–AgX in the presence of 0.1 M $K_4[Fe(CN)_6]$. Adapted from Ref. [120] with permission. Copyright (2017), Talanta. Copyright (2018), Journal of Materials Chemistry B

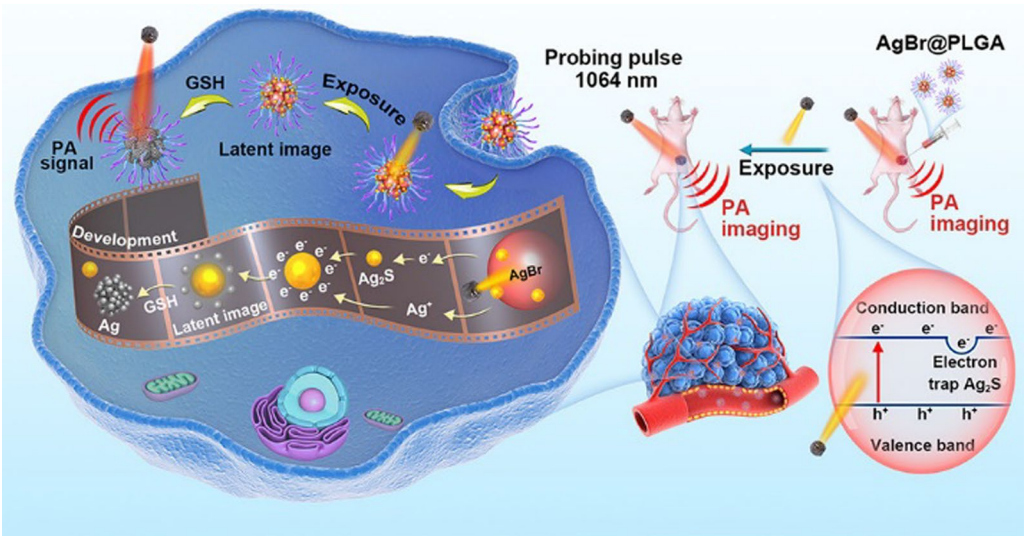

Fig. 7 Synthesis process of the prepared AgBr@PLGA NCs and the schematic illustration that tumor area is graphically fixed via redox reaction where the NIR-transparent AgBr@PLGA NCs can be reduced by the tumor-abundant GSH into strongly absorbing silver NPs. Adapted from Ref. [122] with permission. Copyright (2021), ACS Publications

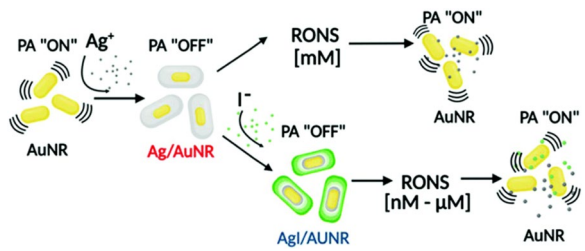

Fig. 8 Schematic of shell optimization. Schematic representation of the current work. Iodide doping results in biologically relevant [nM–µM] sensitivity to RONS. Adapted from Ref. [123] with permission. Copyright (2020), Royal Society of Chemistry

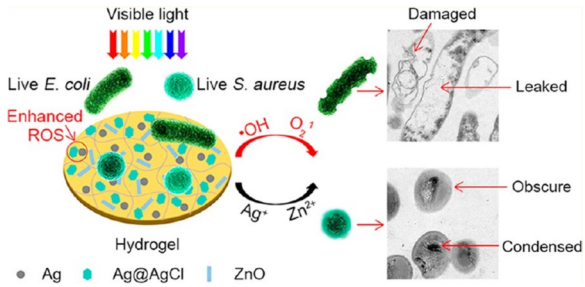

Fig. 9 Mechanism of Ag/Ag@AgCl/ZnO antibacterial. Adapted from Ref. [8] with permission. Copyright (2017) ACS Nano

96-well plate. Then the FA-AgI conjugate was added to the folate receptor, which is a simple binding reaction and no antibodies were involved. Then, taking advantage of the photo-oxidase-like activity of AgI, TMB was added as a substrate. Upon irradiation with visible light ($\lambda \geq 420$ nm), blue-colored TMB oxidation products were formed in the presence of tumor cells.

In 2017, Zhang's group reported a Cu^{2+}-doped Ag–AgI nanocomposite (Cu^{2+}/Ag–AgI), which was designed for photosensitive colorimetric immunoassay for tumor marker detection [120]. Figure 6A clearly shows that it was designed as a highly photosensitive colorimetric immunoassay for carcinoembryonic antigen (CEA) detection based on the Cu^{2+}/Ag–AgI. The Cu^{2+}/Ag–AgI can oxidize TMB, which was synthesized by an impregnation method. After that, they achieved the immune-complex built on the surface of a magnetic bead by utilizing Cu^{2+}/Ag–AgI as labels based on a sandwich-type immunoassay. The blue color of TMB_{ox} was obtained under visible irradiation and ultraviolet spectrum scanning, which showed increased absorbance values with increasing CEA concentrations. Above all, the developed colorimetric immunoassay exhibited good selectivity, repeatability, stability, and possible applications in the real serum sample analysis.

In 2018, Mazhabi et al. reported a C_3N_4–AgI/ITO photoelectrode for specific cervical cancer HeLa cell recognition [121]. They claimed that the C_3N_4–AgI/ITO photoelectrode as a label-free aptamer-based cytosensor can be applied in cancer diagnostics. As a new nanomaterial, the C_3N_4–AgI/ITO photoelectrode has both photoactive and bio-recognition features, which perfectly satisfied the requirements of photoelectrochemical (PEC) biosensors for cancer cell detection. In this study, the authors designed a novel label-free PEC aptamer-based cytosensor for the specific detection of cancer cells such

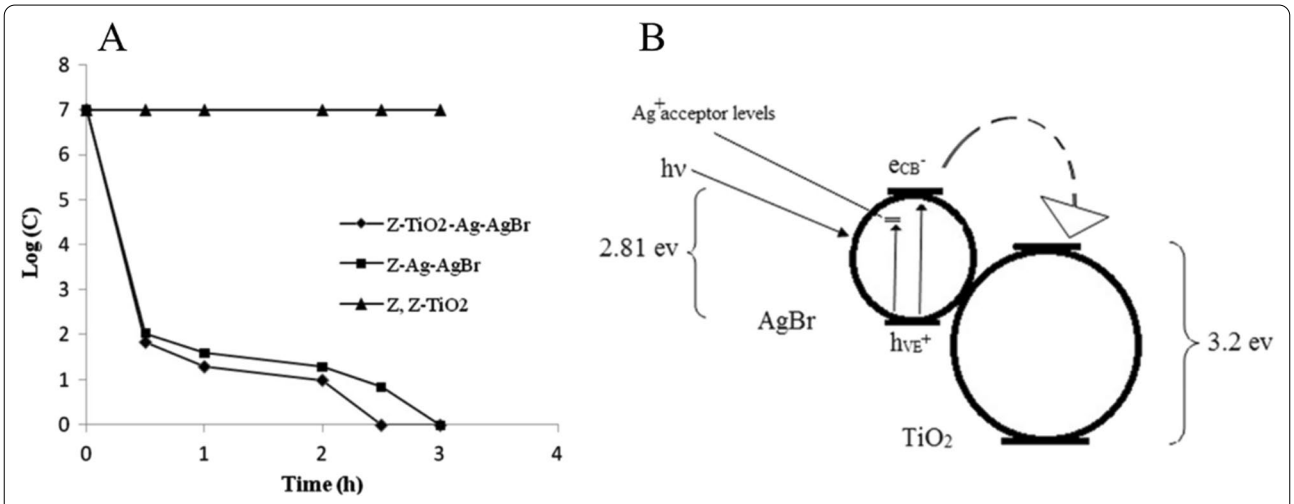

Fig. 10 **A** *E. coli* inactivation curve over the composites at the visible light ($C_0 = 1 \times 10^7$, 30 mL, 12 mg of catalyst). **B** Electrons transfer from AgBr conduction band to the lower position TiO_2 conduction band and delay the electron–hole recombination. Adapted from Ref. [9] with permission. Copyright (2012) Materials Science in Semiconductor Processing

as HeLa cells by using water-dispersible g-C_3N_4–AgI nanocomposites as visible light-sensitive materials and an anti-CEM/PTK7 aptamer as the bio-recognition element. As shown in Fig. 6B, when a suitable amount of AgI NPs was doped in the two-dimensional graphite-like carbon nitride nano-sheets (g-C_3N_4 NSs), the visible light photocurrent response could be significantly improved. The PEC response of the as-prepared biosensor based on the g-C_3N_4–AgI/ITO photoelectrode was linearly proportional to the relevant cancer cells such as HeLa cells in concentrations ranging from 10 to 10^6 cells per mL with a limit of detection of 5 cells per mL. In addition, the g-C_3N_4–AgI/ITO photoelectrode and the fabricated cytosensor exhibited long-term stability, good reproducibility, excellent selectivity, and high sensitivity, demonstrating the successful conjugation of g-C_3N_4–AgI NSs with the aptamer and targeting cancer cells in the high-performance PEC cytosensor.

In 2021, Cui et al. reported that AgBr@PLGA nanocrystals can be applied in ultrahigh-sensitive and tumor-specific photoacoustography in the near-infrared NIR-II region [122]. The highly up-regulated glutathione (GSH) concentration in the tumor microenvironment is generally identified to be an effective endogenous characteristic of cancerous tissues. Therein, an ultrahigh-sensitive and tumor-specific photoacoustography technique in the NIR-II region based on optical writing and redox-responsive chromogenic graphic fixing was developed by introducing a self-synthesized photosensitive silver bromide modified with poly lactic-co-glycolic acid (AgBr@PLGA) nanocrystals. After optically triggered by external light, the NIR-transparent AgBr@PLGA nanocrystals can be reduced by the tumor-abundant GSH into strongly absorbing AgNPs, significantly boosting the "turn-on" photoacoustic (PA) signal in the NIR-II region. As shown in Fig. 7, the tumor area can be graphically fixed and developed in the photoacoustography. Experiments on both in vitro phantoms and in vivo mouse models demonstrated that the tumor area was specifically identified by the photoacoustography with the background signals effectively suppressed by dynamically modulating the exposure time.

Mantri et al. reported that iodide-doped precious metal NPs, such as Ag@AuNR, can be used to measure oxidative stress in vivo via photoacoustic imaging [123]. Since the accumulation of reactive oxygen and nitrogen

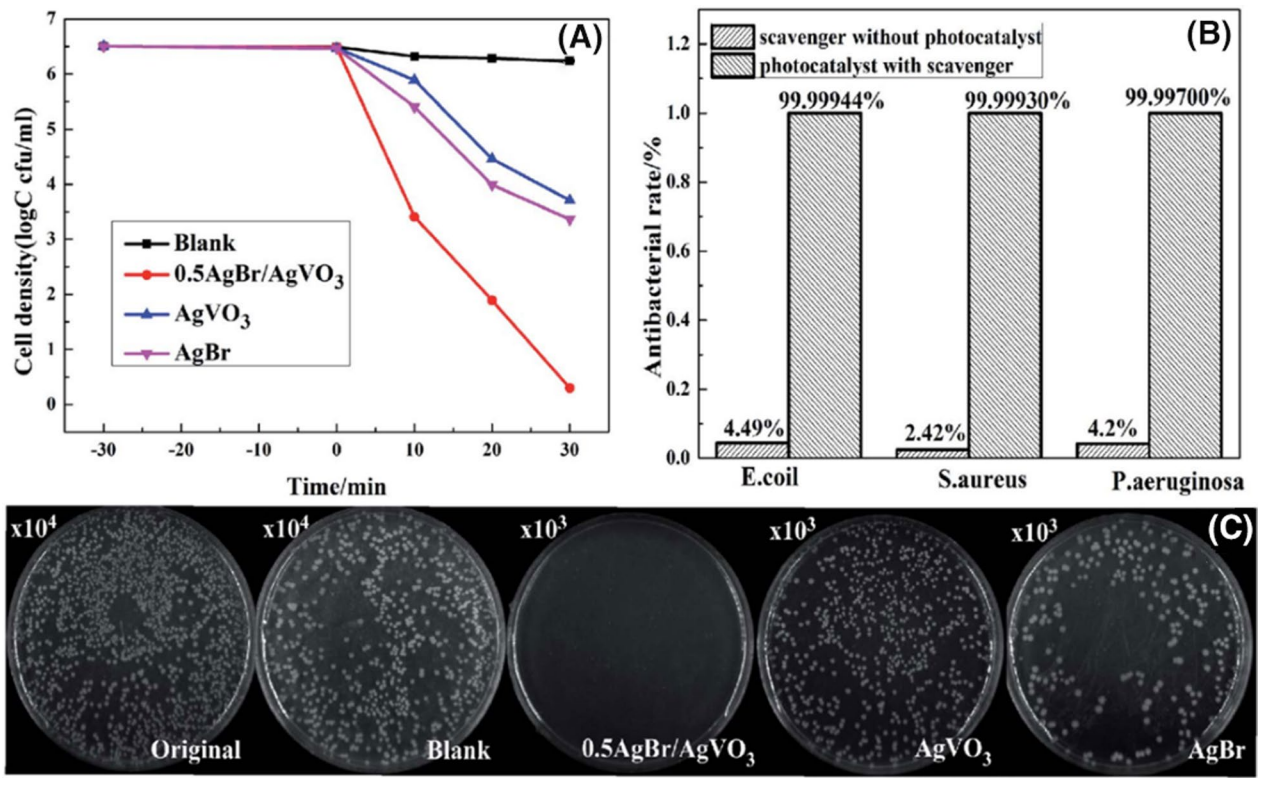

Fig. 11 **A** *P. aeruginosa* survival curves in the antibacterial experiments, **B** photocatalytic antibacterial rates of *E. coli*, *S. aureus* and *P. aeruginosa* with 0.5AgBr/$AgVO_3$ for 30 min, and the survival pictures of *P. aeruginosa* colonies in the presence of different photocatalysts. **C** Copyright (2019). Adapted from Ref. [130] with permission. The Royal Society of Chemistry

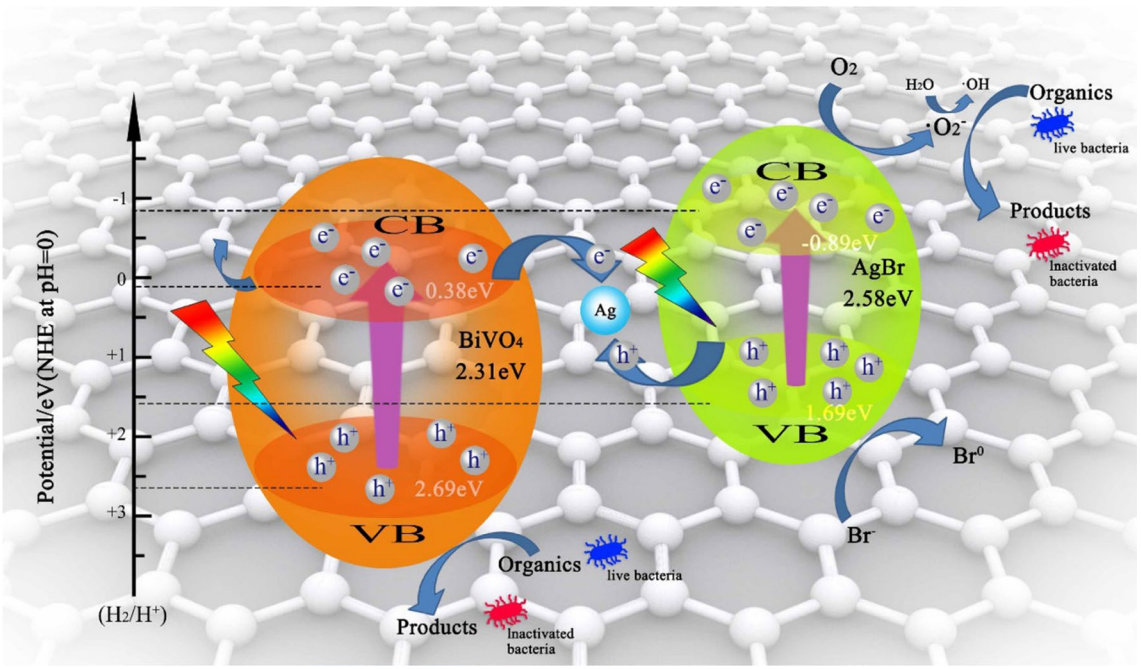

Fig. 12 The proposed tentative mechanism for photocatalytic disinfection of Ag-AgBr/ $BiVO_4$/GA composite under visible light irradiation. Adapted from Ref. [131] with permission. Copyright (2020) Colloids and Surfaces A

species (RONS) can directly influence cell damage and cell death, the measurement of RONS is important for cancer detection. However, both reactive oxygen and nitrogen species are short-lived and exist only in trace amount in vivo (biologically RONS levels are in the nM–μM scale). Therefore, they used halide doping to tune the electrochemical properties of gold-core/silver-shell NPs to match the oxidation potential of RONS. The proposed mechanism is shown in Fig. 8. In this work, the authors provided the synthesis, characterization, and application of these AgI-coated gold nanorods (AgI/AuNR) and discussed that halide doping lowered the reduction potential of Ag, which resulted in a 1000-fold increase in H_2O_2 and 100,000-fold increase in $ONOO^-$ sensitivity. The AgI/AuNR system also etched 45-fold faster than the undoped Ag/AuNR.

AgX-Based Antibacterial Nanomaterials

Bacteria are an important cause of disease and infection. Some microorganisms such as golden staphylococci may cause serious human tissue damage. Thus, the preparation of antibacterial materials has caused widespread interest [6, 124, 125]. One of the well-known applications of AgNPs is antimicrobial. Aside from pure AgNPs, using its AgX hybrid materials has also been reported.

Recently, Ag@AgCl as a highly efficient photocatalyst was applied to the photocatalytic degradation of pollutants and organic synthesis products [63, 126–128]. Since the charge hole combination rate of the AgCl is low under visible light, and the active oxygen species, such as hydroxyl radicals, are relatively high in concentration and are applied to the preparation of antibacterial materials.

In 2017, Mao et al. reported that Ag/Ag@AgCl/ZnO hybrid nanostructures exhibited a high antibacterial efficiency against both *Escherichia coli* (*E. coli*) and Staphylococcus aureus under visible light irradiation (Fig. 9) [8]. In their study, the Ag/Ag@AgCl nanostructures enhanced the antibacterial activity of ZnO. This hydrogel system killed 95.95% of *E. coli* and 98.49% of S. aureus under visible light irradiation after 20 min. In addition, this system provided about 90% Zn^{2+} release in the acidic environment within 3 days, but 10% Zn^{2+} release occurred in the neutral environment within 21 days. The results showed that the release of Ag^+ and Zn^{2+} stimulated the immune function to produce a large number of white blood cells and neutrophils, which resulted in the production of antibacterial effects.

Silver bromide (AgBr) is an n-type photosensitive semiconductor with a 2.6 eV bandgap [61]. Ag/AgBr NPs are applied to the disinfection of bacteria because of the plasma effect and high efficiency charge molecular efficiency under light irradiation [59, 129].

In 2012, Padervand et al. evaluated the photocatalytic activities of zeolite-based Ag/AgBr and Ag/AgBr/TiO_2 photocatalysts for the inactivation of E. coli [9]. In

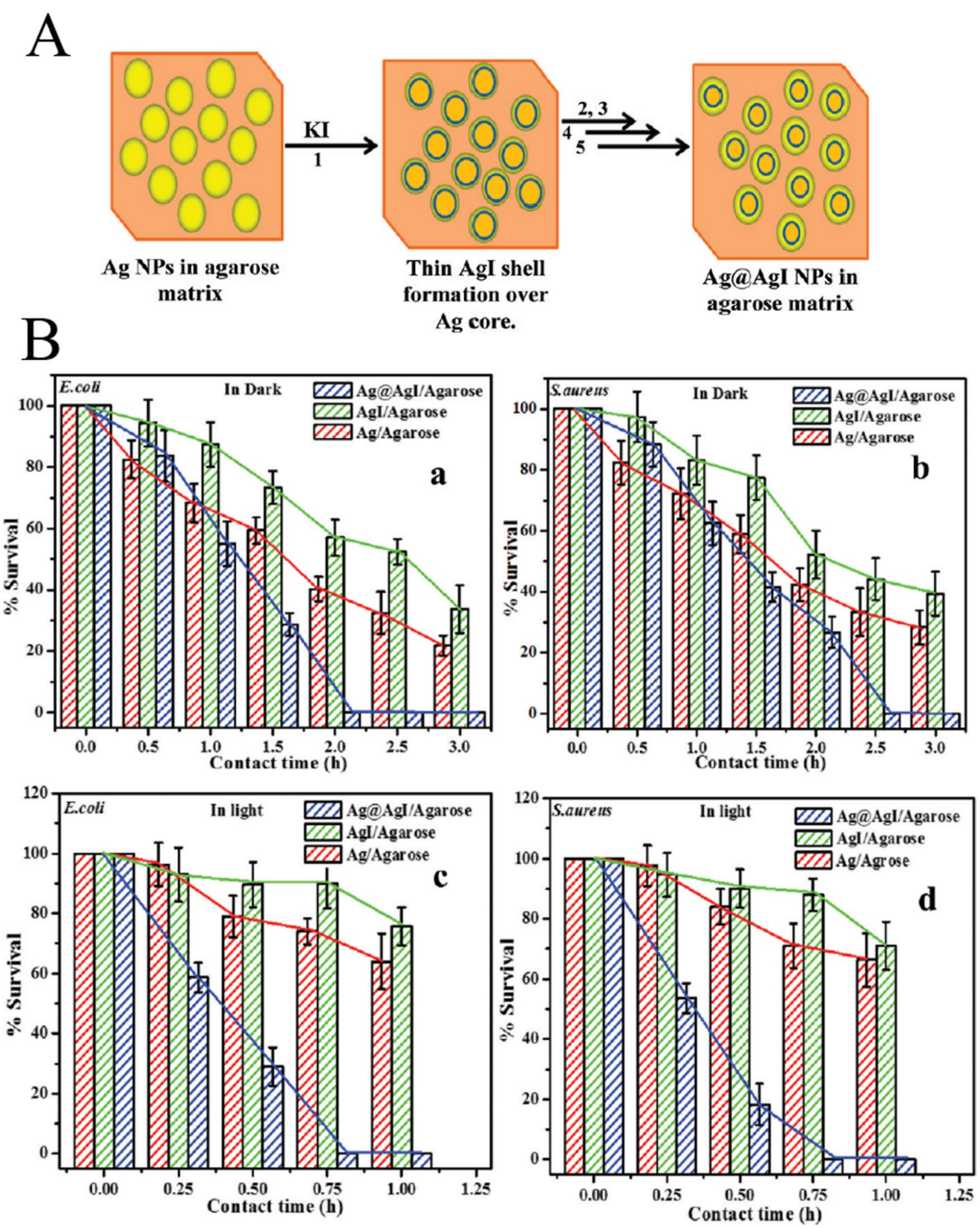

Fig. 13 **A** Schematic illustration of the stepwise formation of core@shell structure of Ag@AgI in agarose matrix. **B** Viable cell count test by nutrient agar plating: percentage survival bacteria versus contact time for (a) *E. coli* and (b) *S. aureus* in the dark, and (c) *E. coli* and (d) *S. aureus* in the presence of light. Adapted from Ref. [7] with permission. Copyright (2012) Langmuir

their study, the Ag/AgBr/zeolite and Ag/AgBr/TiO_2/zeolite had a high activity and decreased *E. coli* concentration most, but the zeolite and TiO_2/zeolite had a lower antibacterial activity (Fig. 10A). After the visible light illumination, the electron–hole pairs of Ag/AgBr/TiO_2/zeolite were generated. The electrons of AgBr conduction

Table 1 The stability of Ag/AgX biosensors

Materials	Methods	Cycles/time	Performance decrease	References
GH/PANI/Ag@AgCl	Degradation efficiency	6 cycles	3%	[139]
AgI/Ag/BiOI	Switching the light source	15 cycles	0%	[140]
CS–AgI/TiO_2	Degradation efficiency	4 cycles	0%	[48]
AgI/CBO/FTO	On/off illumination	5 min	0%	[141]
ITO/g–C_3N_4–AgI	On/off illumination	500 s	2%	[121]
AuNPs–AgCl@PANI	Reduction and oxidation of H_2O_2	7 months	Excellent catalytic effect	[142]

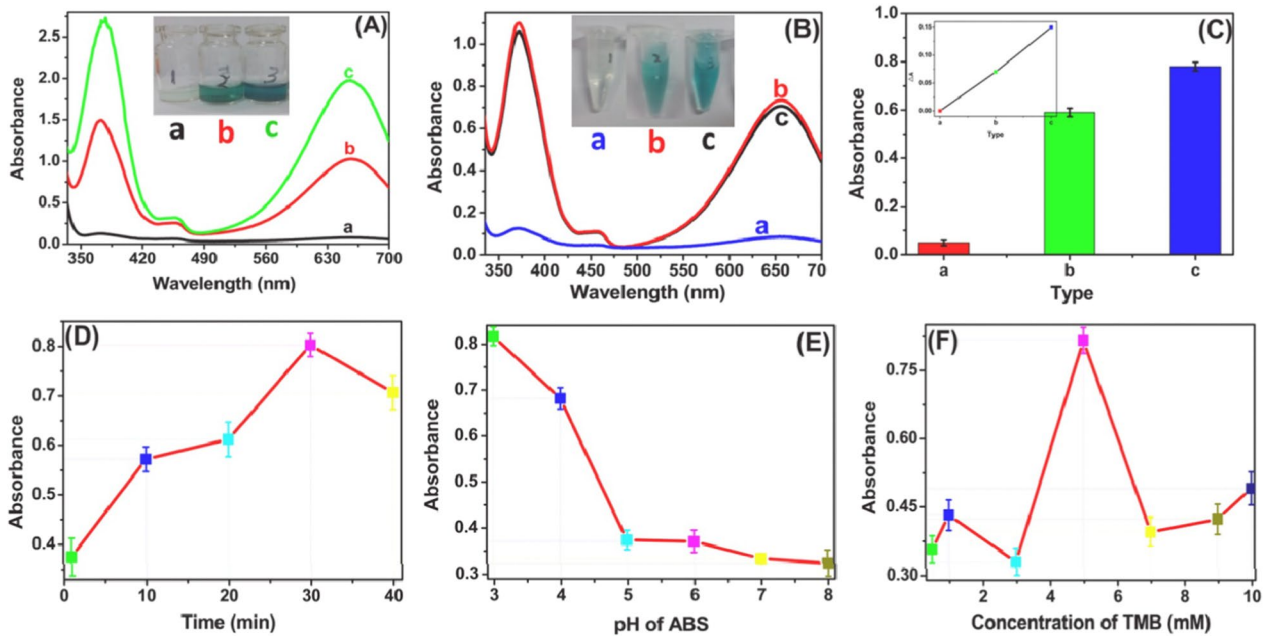

Fig. 14 **A** The UV–Vis spectrums of (a) TiO_2 + TMB, (b) AgI + TMB, and (c) CS-AgI/TiO_2 + TMB under visible light illumination [the inset is the photographs of a, b, c]; **B** The UV–Vis spectrums of (a) Fe_3O_4 + TMB, (b) CS-AgI/TiO_2 + TMB, and (c) Fe_3O_4 + CS–AgI/TiO_2 + TMB; **C** the UV–Vis absorbance of different immunosensors for 0.5 nM CAP (a) anti-CAP-CS-TiO_2/CAP-BSA/MB, (b) anti-CAP-CS-AgI/CAP-BSA/MB, and (c) anti-CAP-CS-AgI/TiO_2/CAP-BSA/MB [the inset is ΔA of a, b, c for 0.5 nM CAP]; The effect of **D** incubation time of antigen–antibody, **E** pH of ABS, and **F** concentration of TMB. Adapted from Ref. [48] with permission. Copyright (2017) Biosensors and Bioelectronics

band can be transferred to TiO_2 conduction band, which is below the AgBr conduction band. This property increased the photoreaction efficiency (Fig. 10B).

In 2019, Zhang et al. reported that AgBr/$AgVO_3$ photocatalysts exhibited enhanced antibacterial efficiency compared to pure AgBr and pure $AgVO_3$ under visible light irradiation [130]. More than 99.9970% of *E. coli*, *S. aureus*, and *P. aeruginosa* cells were killed by the photocatalysis of 0.5AgBr/$AgVO_3$ after 30 min. Overall, the 0.5AgBr/$AgVO_3$ heterojunction photocatalyst had excellent photocatalytic antibacterial performance (Fig. 11).

In 2020, Lin et al. reported a three-dimensional structured Ag-AgBr/$BiVO_4$/graphene aerogel (Ag-AgBr/$BiVO_4$/GA) via a hydrothermal and freeze-drying process [131]. In their study, the Ag-AgBr/$BiVO_4$/GA exhibited a good disinfection performance toward *E. coli* (100% removal rate in 24 min). The proposed photocatalytic mechanism of inactivating *E. coli*/*S. aureus* by Ag-AgBr/$BiVO_4$/GA is presented in Fig. 12. Ag-AgBr/$BiVO_4$/GA was activated to excited states under visible light, and electrons in the valence band of AgBr and $BiVO_4$ were excited to the conduction band (CB). Thus, both two semiconductors can generate electrons and holes. The existence of GA served as an electro-reservoir. Subsequently, the electrons formed in the CB of $BiVO_4$ moved to the AgNPs, and the holes transferred from the VB of the AgBr, which caused the accumulation of electrons in the CB of AgBr and holes in the VB of $BiVO_4$. Finally, the

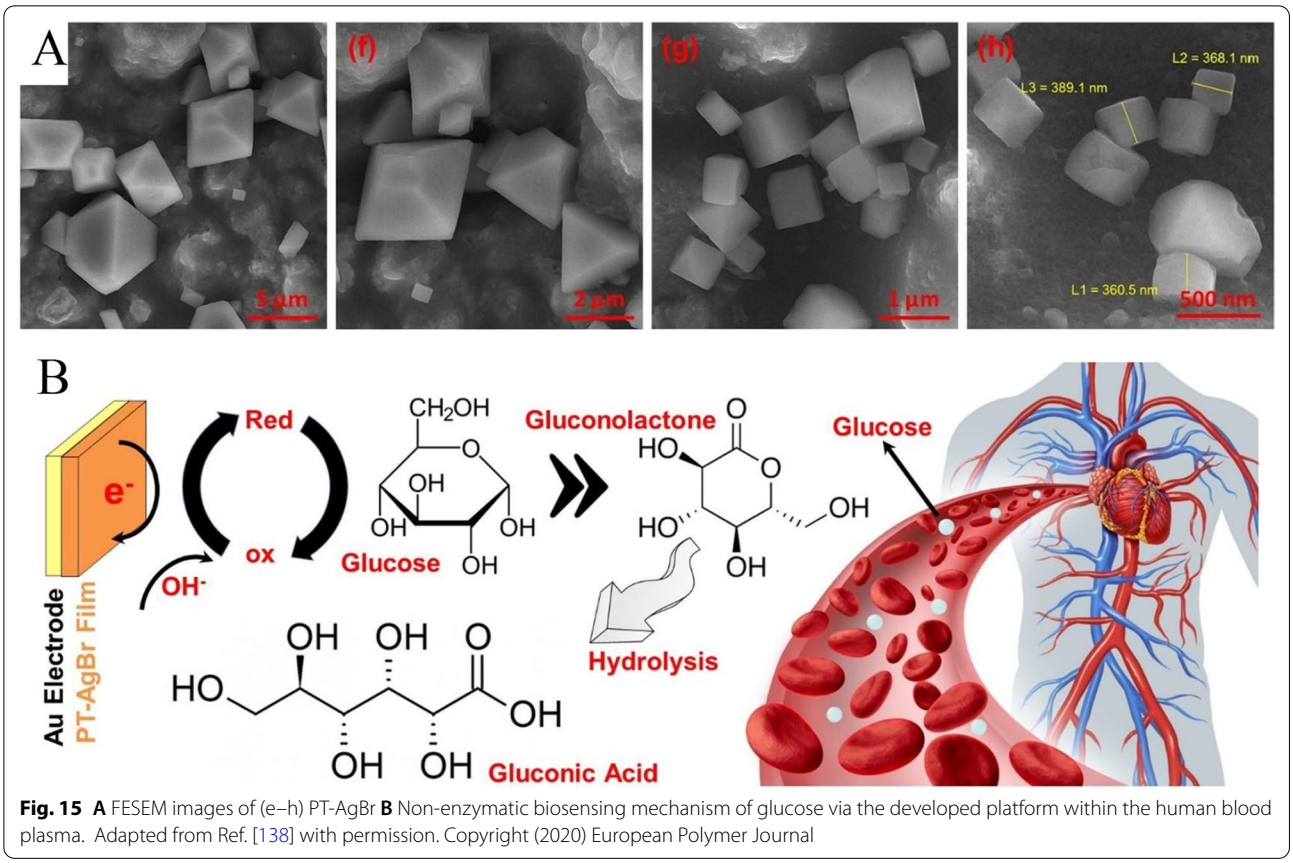

Fig. 15 **A** FESEM images of (e–h) PT-AgBr **B** Non-enzymatic biosensing mechanism of glucose via the developed platform within the human blood plasma. Adapted from Ref. [138] with permission. Copyright (2020) European Polymer Journal

electrons in the CB reacted with O_2 or H_2O to generate active oxygen species, which can oxidize live bacteria into inactive bacteria.

Not only that but AgI can also be used as antibacterial material. In 2012, Ghosh et al. synthesized a core@shell structure consisting of AgNPs and AgI in an agarose matrix (Ag@AgI/agarose), which was an efficient antibacterial agent [7]. In situ synthesis of the catalyst was achieved by adding a low concentration of KI solution gradually. The authors speculated that the AgI thin layer was first formed by AgNPs, and then the AgI layer gradually became thick with the addition of the KI solution (Fig. 13A). Antibacterial studies including repetitive cycles were carried out on Gram-negative *E. coli* and Gram-positive Staphylococcus aureus bacteria in saline water, both in dark and under visible light. The Ag@AgI/agarose could be reused in the antibacterial experiment (Fig. 13B).

AgX-Based Biosensors

A biosensor is a target-specific biomolecule coupled with a signal transduction unit that can be used to identify target analytes with high sensitivity and specificity. AgX has been used to prepare a high sensitivity biosensor, which can detect genes, urine, and blood in humans [132–135]. A recent development is the detection of glucose. Glucose oxidase can oxidize glucose to produce gluconolactone and the reduced enzyme. Subsequently, the reduced enzyme transfers electrons to molecular oxygen in the body's biological fluid to produce hydrogen peroxide (H_2O_2) [136, 137]. Ag/AgX as electrode materials were applied in several biosensor systems because it has good reversibility and its electrode potential is relatively stable [138].

The stability of biosensors is significant to real-world applications. Table 1 summarizes the durability of those Ag/AgX nanomaterials. Most of them used degradation efficiency and control of the light on/off states to test the stability of biosensors.

In 2021, Chen's group reported a new nanomaterial, Ag@AgCl photocatalyst loaded on 3D graphene/PANI hydrogels that can be used for in situ SERS monitoring [139]. With silver halides AgX (X = Cl, Br, I) and the surface plasmon resonance (SPR) of metallic Ag, heterojunctions of Ag@AgX can exhibit high stability and highly efficient utilization of visible light. The authors synthesized GH/PANI/Ag@AgCl nanocomposites by reacting

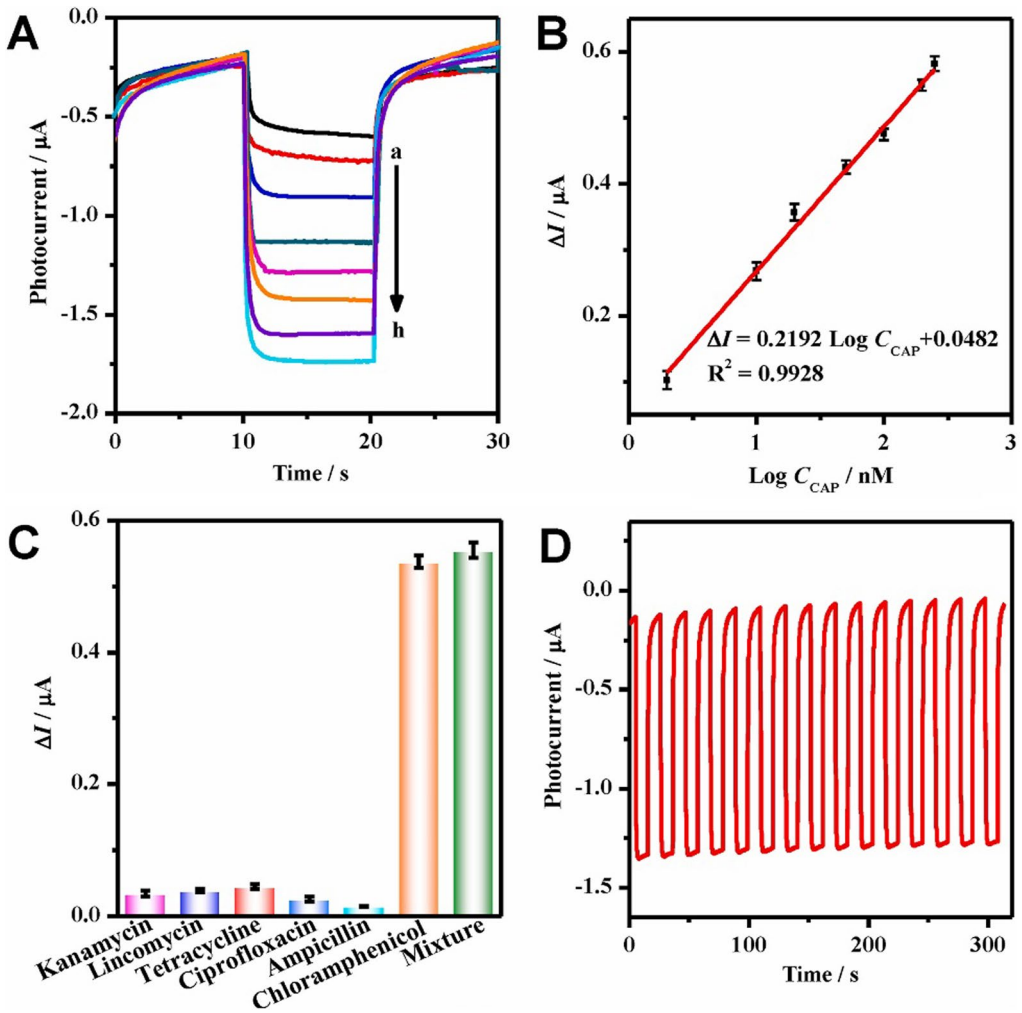

Fig. 16 Photocurrents **A** of the developed PEC aptasensor with different CAP concentrations (curves a–h: 0–250 nM). Calibration curve (**B**). Selectivity (**C**) toward 200 nM CAP with equal amount of the interfering substances (i.e., kanamycin, lincomycin, tetracycline, ciprofloxacin, and ampicillin), and their mixture. Stability (**D**) of the as-fabricated PEC aptasensor. Adapted from Ref. [140] with permission. Copyright (2021) Biosensors and Bioelectronics

Ag^+ ions with the Cl^- in the HCl-doped PANI in 3D GH/PANI and the subsequent photo-assisted reduction. These new nanomaterials have enhanced adsorption-photocatalytic degradation. Due to combining AgNPs with graphene and PANI, it can be applied for real-time SERS detection. Hence, graphene/PANI composites exhibited enhanced electrical conductivity and electrochemical stability compared with bare PANI, which has been widely applied in biosensors because of its optical, electronic, and electrochemical features.

2016, Chang et al. used AgI/TiO_2 hybrid material as a label to produce a color signal with a visible optic excitation for quantitative analysis of chloramphenicol (CAP) (Fig. 14). [48] The enzyme-like catalytic nanomaterials are also known as nanozymes [143–146]. Using a competitive immunoassay with CS-AgI/TiO_2 labeled CAP antibodies as tags, detection of CAP was achieved on the surface of CAP-BSA modified magnetic bead. In this reaction, the participation of hydrogen peroxide was not required [48]. The combination of AgI and TiO_2 effectively reduced the composite of photocarriers and electrons, which greatly enhanced the ability of solution color (Fig. 14A,B). This allowed the immunosensor sensor to have better sensitivity and a low detection limit of 0.03 nM.

In 2020, Hashemi et al. reported that AgBr NPs with the polymeric structure of PT could sense glucose through a real-time and precise approach [138]. In their system, PT-AgBr was modified cubic, anorthic or hybrid cubic–anorthic morphologies (Fig. 15A). They confirmed

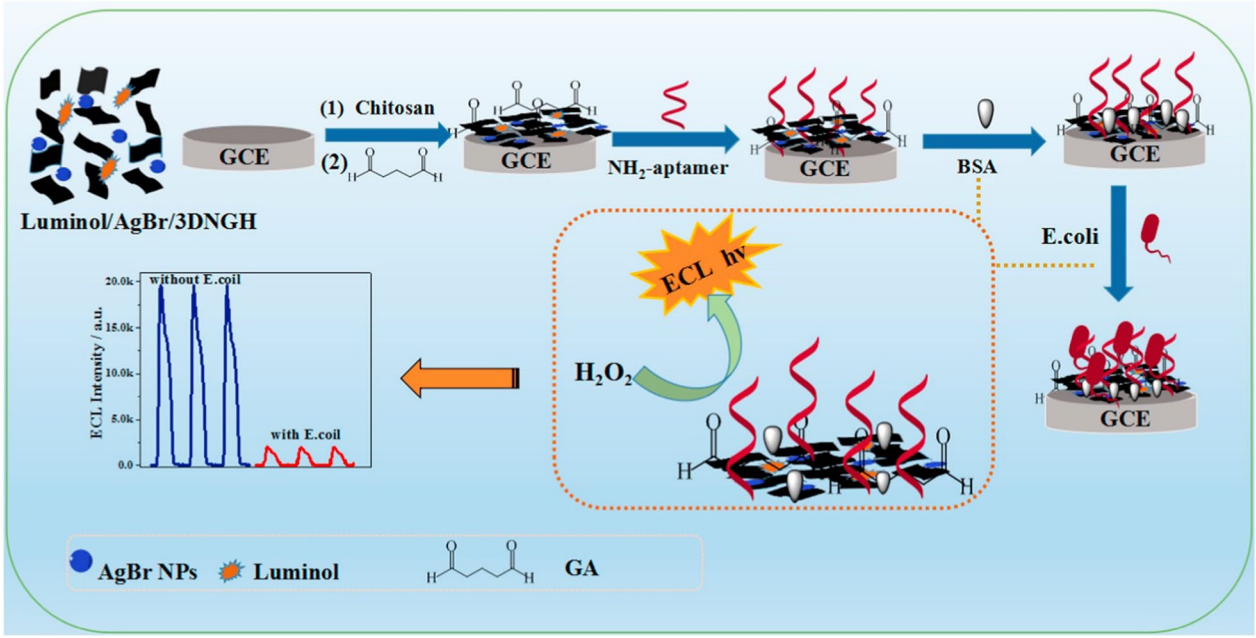

Fig. 17 The schematic presentation for the ECL *Escherichia coli* biosensor fabricated with luminol/AgBr/3DNGH. Adapted from Ref. [147] with permission. Copyright (2017) Biosensors and Bioelectronics

the successful formation of AgBr, PT and PT-AgBr by diverse characterizations, for example, X-ray diffractogram, zeta potential, and FESEM. PT has a conductive polymeric structure. So, its integration with AgBr can improve its electrocatalytic performance, Further, glucose detection can be accurately performed (Fig. 15B), and the PT-AgBr showed zeta potential and electrophoretic mobility of 16.7 mV/0.000129 cm^2/Vs, respectively.

In 2021, Zhu et al. reported that 3D Z-scheme AgI/Ag/BiOI heterojunction for highly sensitive determination of CAP, thereby fabricating a "signal-on" PEC aptasensor [140]. In their study, the AgI/Ag/BiOI photocatalyst was prepared by an ion-exchange and photo-irradiation method, which improved the photocurrents by facilitating the spatial separation of the photo-generated charge carriers. The response of the PEC aptasensor was linearly correlated between the photocurrents and the logarithm of the CAP concentrations, which had the advantages of being sensitive, simple and stable (Fig. 16).

In 2019, Hao et al. reported AgBr NPs-anchored 3D nitrogen-doped graphene hydrogel (3DNGH) nanocomposites with a large surface by hydrothermal method (Fig. 17) [147]. With a porous structure, 3DNGH had a large surface area that can favor the immobilization of AgBr and luminol, where in turn, luminol and hydrogen peroxide can be in close contact. They fabricated all-solid-state luminol electrochemiluminescence *E. coli* aptasensors, which showed great performance. So, the potential for the luminol/AgBr/3DNGH nanocomposite for E. coli detection in biomedical and environmental analysis was developed.

Summary and Perspectives

In this article, we reviewed the biomedical and bioanalytical applications of AgX. Silver halide has been widely used in industry as electrodes (Ag/AgCl), imaging materials (AgBr), and artificial rainfall (AgI).

However, AgX NPs as photocatalytic materials have not been intensively studied because they decompose to produce AgNPs under visible light. Through the combination of silver NPs and silver halide, the decomposition rate of silver halide can be significantly reduced. The principle is that silver halide, as a semiconductor inorganic photocatalyst, will generate photo-generated carriers and generate electrons and holes under visible light irradiation. However, the rate of this process is low because electrons and holes will combine, reducing the occurrence of oxidation reactions. Therefore, the silver elementary substance can be doped into silver halide, because elemental silver, as a precious metal, can produce a surface plasmon effect and promote electron transport. One of the drawbacks is the potential photofatigue effect during long-term irradiation, which may result in a gradual loss of efficiency. The solution is that AgNPs and AgX form a Schottky junction, which reduces the contact between electrons and holes, thereby promoting photocatalytic efficiency and

extending the working life. Based on the above discussion, it is possible to apply Ag/AgX photocatalysts in the fields of cancer treatment, cancer diagnosis, antibacterial, wound healing, and biosensor.

The applications of Ag/AgX in medicine are only at the proof-of-concept stage because the working wavelength for Ag/AgX nanomaterials was almost exclusively in the UV/visible region, and the short-wavelength light can suffer from phototoxicity and poor tissue penetration. To solve this problem, a near-infrared (NIR) light featuring lower toxicity and deeper tissue penetration has more advantages in biological applications. By doping heterojunctions and other methods, the range of photocatalytic wavelengths can be increased, and the energy bandgap can be reduced so that the silver halide nanomaterial can absorb more energy in a broad wavelength range. At the same time, AgX materials also have certain limitations. For example, simple AgX is susceptible to decomposition under strong light, and AgNPs produced by the decomposition have cytotoxicity to human tissues and organs. Therefore, further research on the application of silver halide surface plasma materials in the field of photocatalysis is indispensable.

Acknowledgements
We thank all researchers that discussed and helped us with this review.

Author contributions
LZ contributed to conceptualization, investigation of these related articles and journals, formal analysis, summary, and writing of the original draft. HZ reviewed and edited the final draft and supervised the study. All authors read and approved the final manuscript.

Funding
Not applicable.

Availability of data and material
The datasets used or analyzed during the study are available from the related journals and the corresponding author upon reasonable request.

Declarations

Ethics approval and consent to participate
Not applicable.

Consent for publication
All authors gave their consent for publication.

Competing interests
The authors declare that they have no competing interests.

Received: 23 July 2022 Accepted: 19 November 2022
Published online: 28 November 2022

References

1. Christensen L, Vivekanandhan S, Misra M, Kumar Mohanty A (2011) Biosynthesis of silver nanoparticles using Murraya koenigii (curry leaf): an investigation on the effect of broth concentration in reduction mechanism and particle size. Adv Mater Lett 2(6):429–434
2. Morones JR, Elechiguerra JL, Camacho A, Holt K, Kouri JB, Ramírez JT et al (2005) The bactericidal effect of silver nanoparticles. Nanotechnology 16(10):2346
3. Naik RR, Stringer SJ, Agarwal G, Jones SE, Stone MO (2002) Biomimetic synthesis and patterning of silver nanoparticles. Nat Mater 1(3):169–172
4. Rai M, Yadav A, Gade A (2009) Silver nanoparticles as a new generation of antimicrobials. Biotechnol Adv 27(1):76–83
5. Kim C, Jeon HS, Eom T, Jee MS, Kim H, Friend CM et al (2015) Achieving selective and efficient electrocatalytic activity for CO_2 reduction using immobilized silver nanoparticles. J Am Chem Soc 137(43):13844–13850
6. Brogden KA (2005) Antimicrobial peptides: Pore formers or metabolic inhibitors in bacteria? Nat Rev Microbiol 3(3):238–250
7. Ghosh S, Saraswathi A, Indi SS, Hoti SL, Vasan HN (2012) Ag@AgI, core@shell structure in agarose matrix as hybrid: synthesis, characterization, and antimicrobial activity. Langmuir 28(22):8550–8561
8. Mao C, Xiang Y, Liu X, Cui Z, Yang X, Yeung KWK et al (2017) Photo-inspired antibacterial activity and wound healing acceleration by hydrogel embedded with Ag/Ag@AgCl/ZnO nanostructures. ACS Nano 11(9):9010–9021
9. Padervand M, Elahifard MR, Meidanshahi RV, Ghasemi S, Haghighi S, Gholami MR (2012) Investigation of the antibacterial and photocatalytic properties of the zeolitic nanosized AgBr/TiO_2 composites. Mater Sci Semicond Process 15(1):73–79
10. Setterington EB, Alocilja EC (2012) Electrochemical biosensor for rapid and sensitive detection of magnetically extracted bacterial pathogens. Biosensors 2(1):15–31
11. Du P, Niu Q, Chen J, Chen Y, Zhao J, Lu X (2020) "Switch-On" fluorescence detection of glucose with high specificity and sensitivity based on silver nanoparticles supported on porphyrin metal–organic frameworks. Anal Chem 92(11):7980–7986
12. Dwivedi P, Narvi SS, Tewari RP (2012) Rudraksha assisted generation of silver nanoparticles for integrated application in the biomedical landscape. Int J Green Nanotechnol 4(3):248–261
13. Shang L, Qin C, Jin L, Wang L, Dong S (2009) Turn-on fluorescent detection of cyanide based on the inner filter effect of silver nanoparticles. Analyst 134(7):1477–1482
14. Dankovich TA, Gray DG (2011) Bactericidal paper impregnated with silver nanoparticles for point-of-use water treatment. Environ Sci Technol 45(5):1992–1998
15. Kallman EN, Oyanedel Craver VA, Smith JA (2011) Ceramic filters impregnated with silver nanoparticles for point-of-use water treatment in rural Guatemala. J Environ Eng 137(6):407–415
16. Morsi RE, Alsabagh AM, Nasr SA, Zaki MM (2017) Multifunctional nanocomposites of chitosan, silver nanoparticles, copper nanoparticles and carbon nanotubes for water treatment: antimicrobial characteristics. Int J Biol Macromol 97:264–269
17. Carbone M, Donia DT, Sabbatella G, Antiochia R (2016) Silver nanoparticles in polymeric matrices for fresh food packaging. J King Saud Univ Sci 28(4):273–279
18. De Moura MR, Mattoso LH, Zucolotto V (2012) Development of cellulose-based bactericidal nanocomposites containing silver nanoparticles and their use as active food packaging. J Food Eng 109(3):520–524
19. Kumar S, Shukla A, Baul PP, Mitra A, Halder D (2018) Biodegradable hybrid nanocomposites of chitosan/gelatin and silver nanoparticles for active food packaging applications. Food Packag Shelf Life 16:178–184
20. Chhipa H (2017) Nanofertilizers and nanopesticides for agriculture. Environ Chem Lett 15(1):15–22
21. Kashyap PL, Kumar S, Srivastava AK, Sharma AK (2013) Myconanotechnology in agriculture: a perspective. World J Microbiol Biotechnol 29(2):191–207
22. Mishra S, Singh H (2015) Biosynthesized silver nanoparticles as a nanoweapon against phytopathogens: exploring their scope and potential in agriculture. Appl Microbiol Biotechnol 99(3):1097–1107
23. Sujatha J, Suriya P, Rajeshkumar S (2017) Biosynthesis and characterization of silver nanoparticles by actinomycetes isolated from agriculture field and its application on antimicrobial activity. Res J Pharm Technol 10(6):1963–1968

24. Alarcon E, Vulesevic B, Argawal A, Ross A, Bejjani P, Podrebarac J et al (2016) Coloured cornea replacements with anti-infective properties: expanding the safe use of silver nanoparticles in regenerative medicine. Nanoscale 8(12):6484–6489
25. Shenava A, Sharma SM, Shetty V, Shenoy S (2015) Silver nanoparticles: a boon in clinical medicine. J Oral Res Rev 7(1):35
26. Singh M, Singh S, Prasad S, Gambhir I (2008) Nanotechnology in medicine and antibacterial effect of silver nanoparticles. Dig J Nanomater Biostruct 3(3):115–122
27. Wong KK, Liu X (2010) Silver nanoparticles—The real "silver bullet" in clinical medicine? MedChemComm 1(2):125–131
28. Awazu K, Fujimaki M, Rockstuhl C, Tominaga J, Murakami H, Ohki Y et al (2008) A plasmonic photocatalyst consisting of silver nanoparticles embedded in titanium dioxide. J Am Chem Soc 130(5):1676–1680
29. Sarina S, Waclawik ER, Zhu H (2013) Photocatalysis on supported gold and silver nanoparticles under ultraviolet and visible light irradiation. Green Chem 15(7):1814–1833
30. Khatoon N, Mazumder JA, Sardar M (2017) Biotechnological applications of green synthesized silver nanoparticles. J Nanosci Curr Res 2(107):2572–0813
31. Sheikh FA, Barakat NA, Kanjwal MA, Chaudhari AA, Jung I-H, Lee JH et al (2009) Electrospun antimicrobial polyurethane nanofibers containing silver nanoparticles for biotechnological applications. Macromol Res 17(9):688–696
32. Sheikh FA, Barakat NA, Kanjwal MA, Jeon SH, Kang HS, Kim HY (2010) Self synthesize of silver nanoparticles in/on polyurethane nanofibers: nano-biotechnological approach. J Appl Polym Sci 115(6):3189–3198
33. AbuMousa RA, Baig U, Gondal MA, AlSalhi MS, Alqahtani FY, Akhtar S et al (2018) Photo-catalytic killing of HeLa cancer cells using facile synthesized pure and Ag loaded WO_3 nanoparticles. Sci Rep 8(1):15224
34. Dhanalekshmi KI, Magesan P, Sangeetha K, Zhang X, Jayamoorthy K, Srinivasan N (2019) Preparation and characterization of core-shell type Ag@SiO nanoparticles for photodynamic cancer therapy. Photodiagn Photodyn Ther 28:324–329
35. Maji SK, Kim DH (2018) $AgInS_2$-coated upconversion nanoparticle as a photocatalyst for near-infrared light-activated photodynamic therapy of cancer cells. ACS Appl Bio Mater 1(5):1628–1638
36. Wang Q, Wang C, Wang X, Zhang Y, Wu Y, Dong C et al (2019) Construction of CPs@MnO-AgNPs as a multifunctional nanosensor for glutathione sensing and cancer theranostics. Nanoscale 11(40):18845–18853
37. Yang L, Kim TH, Cho HY, Luo J, Lee JM, Chueng STD, et al (2020) Hybrid graphene-gold nanoparticle-based nucleic acid conjugates for cancer-specific multimodal imaging and combined therapeutics. Adv Funct Mater
38. Chattopadhyay S, Lo HC, Hsu CH, Chen LC, Chen KH (2005) Surface-enhanced Raman spectroscopy using self-assembled silver nanoparticles on silicon nanotips. Chem Mater 17(3):553–559
39. Emory SR, Nie S (1997) Near-field surface-enhanced Raman spectroscopy on single silver nanoparticles. Anal Chem 69(14):2631–2635
40. Stamplecoskie KG, Scaiano JC, Tiwari VS, Anis H (2011) Optimal size of silver nanoparticles for surface-enhanced Raman spectroscopy. J Phys Chem C 115(5):1403–1409
41. Defnet PA, Anderson TJ, Zhang B (2020) Stochastic collision electrochemistry of single silver nanoparticles. Curr Opin Electrochem 22:129–135
42. Ivanova OS, Zamborini FP (2010) Size-dependent electrochemical oxidation of silver nanoparticles. J Am Chem Soc 132(1):70–72
43. Rodriguez-Sanchez L, Blanco MC, López-Quintela MA (2000) Electrochemical synthesis of silver nanoparticles. J Phys Chem B 104(41):9683–9688
44. Zhou YG, Rees NV, Compton RG (2011) The electrochemical detection and characterization of silver nanoparticles in aqueous solution. Angew Chem Int Ed 50(18):4219–4221
45. Patlolla AK, Berry A, May L, Tchounwou PB (2012) Genotoxicity of silver nanoparticles in *Vicia faba*: a pilot study on the environmental monitoring of nanoparticles. Int J Environ Res Public Health 9(5):1649–1662
46. Stensberg MC, Wei Q, McLamore ES, Porterfield DM, Wei A, Sepúlveda MS (2011) Toxicological studies on silver nanoparticles: challenges and opportunities in assessment, monitoring and imaging. Nanomedicine 6(5):879–898
47. Yu SJ, Yin YG, Liu JF (2013) Silver nanoparticles in the environment. Environ Sci Process Impacts 15(1):78–92
48. Chang H, Lv J, Zhang H, Zhang B, Wei W, Qiao Y (2017) Photoresponsive colorimetric immunoassay based on chitosan modified AgI/TiO_2 heterojunction for highly sensitive chloramphenicol detection. Biosens Bioelectron 87:579–586
49. Zhu X, Liang X, Wang P, Dai Y, Huang B (2018) Porous Ag-ZnO microspheres as efficient photocatalyst for methane and ethylene oxidation: Insight into the role of Ag particles. Appl Surf Sci 456:493–500
50. Ziashahabi A, Prato M, Dang Z, Poursalehi R, Naseri N (2019) The effect of silver oxidation on the photocatalytic activity of Ag/ZnO hybrid plasmonic/metal-oxide nanostructures under visible light and in the dark. Sci Rep 9(1):11839
51. Li H, Jiang D, Huang Z, He K, Zeng G, Chen A et al (2019) Preparation of silver-nanoparticle-loaded magnetic biochar/poly(dopamine) composite as catalyst for reduction of organic dyes. J Colloid Interface Sci 555:460–469
52. Kumari S, Sharma P, Yadav S, Kumar J, Vij A, Rawat P et al (2020) A novel synthesis of the graphene oxide-silver (GO-Ag) nanocomposite for unique physiochemical applications. ACS Omega 5(10):5041–5047
53. Chen S, Quan Y, Yu YL, Wang JH (2017) Graphene quantum dot/silver nanoparticle hybrids with oxidase activities for antibacterial application. ACS Biomater Sci Eng 3(3):313–321
54. Cai B, Wang J, Gan S, Han D, Wu Z, Niu L (2014) A distinctive red Ag/AgCl photocatalyst with efficient photocatalytic oxidative and reductive activities. J Mater Chem A 2(15):5280–5286
55. Dong R, Tian B, Zeng C, Li T, Wang T, Zhang J (2012) Ecofriendly synthesis and photocatalytic activity of uniform cubic Ag@AgCl plasmonic photocatalyst. J Phys Chem C 117(1):213–220
56. Pratap Reddy M, Venugopal A, Subrahmanyam M (2007) Hydroxyapatite-supported Ag-TiO_2 as *Escherichia coli* disinfection photocatalyst. Water Res 41(2):379–386
57. Wang P, Huang B, Lou Z, Zhang X, Qin X, Dai Y et al (2010) Synthesis of highly efficient Ag@ AgCl plasmonic photocatalysts with various structures. Chem Eur J 16(2):538–544
58. Wang P, Huang B, Qin X, Zhang X, Dai Y, Wei J et al (2008) Ag@AgCl: a highly efficient and stable photocatalyst active under visible light. Angew Chem Int Ed Engl 47(41):7931–7933
59. Wang P, Huang B, Zhang Q, Zhang X, Qin X, Dai Y et al (2010) Highly efficient visible light plasmonic photocatalyst Ag@ Ag (Br, I). Chem Eur J 16(33):10042–10047
60. Yan Q, Sun M, Yan T, Li M, Yan L, Wei D et al (2015) Fabrication of a heterostructured Ag/AgCl/Bi_2MoO_6 plasmonic photocatalyst with efficient visible light activity towards dyes. RSC Adv 5(22):17245–17252
61. Yang Y, Guo W, Guo Y, Zhao Y, Yuan X, Guo Y (2014) Fabrication of Z-scheme plasmonic photocatalyst Ag@ AgBr/g-C_3N_4 with enhanced visible-light photocatalytic activity. J Hazard Mater 271:150–159
62. Gamage McEvoy J, Bilodeau DA, Cui W, Zhang Z (2013) Visible-light-driven inactivation of *Escherichia coli* K-12 using an Ag/AgCl–activated carbon composite photocatalyst. J Photochem Photobiol A Chem 267:25–34
63. Wu YA, Li L, Li Z, Kinaci A, Chan MKY, Sun Y et al (2016) Visualizing redox dynamics of a single Ag/AgCl heterogeneous nanocatalyst at atomic resolution. ACS Nano 10(3):3738–3746
64. Zeng C, Hu Y, Guo Y, Zhang T, Dong F, Zhang Y et al (2016) Facile in situ self-sacrifice approach to ternary hierarchical architecture Ag/AgX (X = Cl, Br, I)/$AgIO_3$ distinctively promoting visible-light photocatalysis with composition-dependent mechanism. ACS Sustain Chem Eng 4(6):3305–3315
65. Ghaly HA, El-Kalliny AS, Gad-Allah TA, Abd El-Sattar NEA, Souaya ER (2017) Stable plasmonic Ag/AgCl–polyaniline photoactive composite for degradation of organic contaminants under solar light. RSC Adv 7(21):12726–12736
66. Jin C, Liu X, Tan L, Cui Z, Yang X, Zheng Y et al (2018) Ag/AgBr-loaded mesoporous silica for rapid sterilization and promotion of wound healing. Biomater Sci 6(7):1735–1744
67. Tao S, Yang M, Chen H, Zhao S, Chen G (2018) Continuous synthesis of Ag/AgCl/ZnO composites using flow chemistry and photocatalytic application. Ind Eng Chem Res 57(9):3263–3273

68. Zhang X, Wang P, Meng W, Cui E, Zhang Q, Wang Z et al (2022) Photococatalytic anticancer performance of naked Ag/AgCl nanoparticles. Chem Eng J 428:131265
69. Brewer PJ, Leese RJ, Brown RJ (2012) An improved approach for fabricating Ag/AgCl reference electrodes. Electrochim Acta 71:252–257
70. Kang M, Deng Y, Oderinde O, Su F, Ma W, Yao F et al (2019) Sunlight-driven photochromic hydrogel based on silver bromide with antibacterial property and non-cytotoxicity. Chem Eng J 375:121994
71. Subbaiya R, Saravanan M, Priya AR, Shankar KR, Selvam M, Ovais M et al (2017) Biomimetic synthesis of silver nanoparticles from *Streptomyces atrovirens* and their potential anticancer activity against human breast cancer cells. IET Nanobiotechnol 11(8):965–972
72. Su H, Liu T, Huang L, Huang J, Cao J, Yang H et al (2018) Plasmonic Janus hybrids for the detection of small metabolites. J Mater Chem B 6(44):7280–7287
73. Fayed AS, Youssif RM, Salama NN, Elzanfaly ES, Hendawy HA (2021) Utility of silver-nanoparticles for nano spectrofluorimetric determination of meropenem and ertapenem: bio-analytical validation. Spectrochim Acta Part A Mol Biomol Spectrosc 262:120077
74. Chen Y, Shen C, Wang J, Xiao G, Luo G (2018) Green synthesis of Ag–TiO_2 supported on porous glass with enhanced photocatalytic performance for oxidative desulfurization and removal of dyes under visible light. ACS Sustain Chem Eng 6(10):13276–13286
75. Liao W, Zhang Y, Zhang M, Murugananthan M, Yoshihara S (2013) Photoelectrocatalytic degradation of microcystin-LR using Ag/AgCl/TiO_2 nanotube arrays electrode under visible light irradiation. Chem Eng J 231:455
76. Wang D, Li Y, Li Puma G, Wang C, Wang P, Zhang W et al (2015) Mechanism and experimental study on the photocatalytic performance of Ag/AgCl @ chiral TiO_2 nanofibers photocatalyst: the impact of wastewater components. J Hazard Mater 285:277–284
77. Victora R (1997) Calculated electronic structure of silver halide crystals. Phys Rev B 56(8):4417
78. Dai YD, Lyu RJ, Wu T, Huang CC, Lin Y-W (2020) Influences of silver halides AgX (X= Cl, Br, and I) on magnesium bismuth oxide photocatalyst in methylene blue degradation under visible light irradiation. J Photochem Photobiol A 397:112585
79. Fan Y, Han D, Song Z, Sun Z, Dong X, Niu L (2018) Regulations of silver halide nanostructure and composites on photocatalysis. Adv Compos Hybrid Mater 1(2):269–299
80. Thakur P, Raizada P, Singh P, Kumar A, Khan AAP, Asiri AM (2020) Exploring recent advances in silver halides and graphitic carbon nitride-based photocatalyst for energy and environmental applications. Arab J Chem 13(11):8271–8300
81. Huang S, Xu Y, Xie M, Ma Y, Yan J, Li Y et al (2018) Multifunctional C-doped $CoFe_2O_4$ material as cocatalyst to promote reactive oxygen species generation over magnetic recyclable C-CoFe/Ag–AgX photocatalysts. ACS Sustain Chem Eng 6(9):11968–11978
82. Liu Y, Zeng X, Hu X, Xia Y, Zhang X (2021) Solar-driven photocatalytic disinfection over 2D semiconductors: the generation and effects of reactive oxygen species. Solar Rrl 5(6):2000594
83. Ha M, Kim JH, You M, Li Q, Fan C, Nam JM (2019) Multicomponent plasmonic nanoparticles: from heterostructured nanoparticles to colloidal composite nanostructures. Chem Rev 119(24):12208–12278
84. Hu C, Peng T, Hu X, Nie Y, Zhou X, Qu J et al (2010) Plasmon-induced photodegradation of toxic pollutants with Ag—AgI/Al_2O_3 under visible-light irradiation. J Am Chem Soc 132(2):857–862
85. Liu Y, Zhang K, Tian X, Zhou L, Liu J, Liu B (2021) Quantitative single-particle fluorescence imaging elucidates semiconductor shell influence on Ag@TiO_2 photocatalysis. ACS Appl Mater Interfaces 13(6):7680–7687
86. Temerov F, Pham K, Juuti P, Mäkelä JM, Grachova EV, Kumar S et al (2020) Silver-decorated TiO_2 inverse opal structure for visible light-induced photocatalytic degradation of organic pollutants and hydrogen evolution. ACS Appl Mater Interfaces 12(37):41200–41210
87. Wen XJ, Shen CH, Fei ZH, Fang D, Liu ZT, Dai JT et al (2020) Recent developments on AgI based heterojunction photocatalytic systems in photocatalytic application. Chem Eng J 383:123083
88. Sherry LJ, Chang SH, Schatz GC, Van Duyne RP, Wiley BJ, Xia Y (2005) Localized surface plasmon resonance spectroscopy of single silver nanocubes. Nano Lett 5(10):2034–2038
89. Sherry LJ, Jin R, Mirkin CA, Schatz GC, Van Duyne RP (2006) Localized surface plasmon resonance spectroscopy of single silver triangular nanoprisms. Nano Lett 6(9):2060–2065
90. Zhang H, Itoi T, Konishi T, Izumi Y (2019) Dual photocatalytic roles of light: charge separation at the band gap and heat via localized surface plasmon resonance to convert CO_2 into CO over silver–zirconium oxide. J Am Chem Soc 141(15):6292–6301
91. Chen YZ, Li WH, Li L, Wang LN (2018) Progress in organic photocatalysts. Rare Met 37(1):1–12
92. Fukuzumi S, Ohkubo K (2013) Selective photocatalytic reactions with organic photocatalysts. Chem Sci 4(2):561–574
93. Liu H, Xu C, Li D, Jiang HL (2018) Photocatalytic hydrogen production coupled with selective benzylamine oxidation over MOF composites. Angew Chem 130(19):5477–5481
94. Sung H, Ferlay J, Siegel RL, Laversanne M, Soerjomataram I, Jemal A et al (2021) Global cancer statistics 2020: GLOBOCAN estimates of incidence and mortality worldwide for 36 cancers in 185 countries. CA Cancer J Clin 71(3):209–249
95. Farooq MA, Aquib M, Farooq A, Haleem Khan D, Joelle Maviah MB, Sied Filli M et al (2019) Recent progress in nanotechnology-based novel drug delivery systems in designing of cisplatin for cancer therapy: an overview. Artif Cells Nanomed Biotechnol 47(1):1674–1692
96. Jahanban-Esfahlan R, Seidi K, Banimohamad-Shotorbani B, Jahanban-Esfahlan A, Yousefi B (2018) Combination of nanotechnology with vascular targeting agents for effective cancer therapy. J Cell Physiol 233(4):2982–2992
97. Song W, Anselmo AC, Huang L (2019) Nanotechnology intervention of the microbiome for cancer therapy. Nat Nanotechnol 14(12):1093–1103
98. Zhao CY, Cheng R, Yang Z, Tian ZM (2018) Nanotechnology for cancer therapy based on chemotherapy. Molecules 23(4):826
99. Fan W, Yung B, Huang P, Chen X (2017) Nanotechnology for multimodal synergistic cancer therapy. Chem Rev 117(22):13566–13638
100. Misra R, Acharya S, Sahoo SK (2010) Cancer nanotechnology: application of nanotechnology in cancer therapy. Drug Discov Today 15(19–20):842–850
101. Wang X, Yang L, Chen Z, Shin DM (2008) Application of nanotechnology in cancer therapy and imaging. CA Cancer J Clin 58(2):97–110
102. Bonnett R (1995) Photosensitizers of the porphyrin and phthalocyanine series for photodynamic therapy. Chem Soc Rev 24(1):19–33
103. Loschenov V, Konov V, Prokhorov A (2000) Photodynamic therapy and fluorescence diagnostics. Laser Phys Lawrence 10(6):1188–1207
104. O'Connor AE, Gallagher WM, Byrne AT (2009) Porphyrin and nonporphyrin photosensitizers in oncology: preclinical and clinical advances in photodynamic therapy. Photochem Photobiol 85(5):1053–1074
105. Agostinis P, Berg K, Cengel KA, Foster TH, Girotti AW, Gollnick SO et al (2011) Photodynamic therapy of cancer: an update. CA Cancer J Clin 61(4):250–281
106. Berlien HP (2016) Photodynamic therapy (PDT). J Biophotonics 9(11–12):1300–1301
107. Joseph B, Janam P, Narayanan S, Anil S (2017) Is antimicrobial photodynamic therapy effective as an adjunct to scaling and root planing in patients with chronic periodontitis? A systematic review. Biomolecules 7(4)
108. Rivas Aiello MB, Castrogiovanni D, Parisi J, Azcarate JC, Garcia Einschlag FS, Gensch T et al (2018) Photodynamic therapy in HeLa cells incubated with riboflavin and pectin-coated silver nanoparticles. Photochem Photobiol 94(6):1159–1166
109. Wysocka-Król K, Olsztyńska-Janus S, Plesch G, Plecenik A, Podbielska H, Bauer J (2018) Nano-silver modified silica particles in antibacterial photodynamic therapy. Appl Surf Sci 461:260–268
110. Donohoe C, Senge MO, Arnaut LG, Gomes-da-Silva LC (2019) Cell death in photodynamic therapy: from oxidative stress to anti-tumor immunity. Biochim Biophys Acta Rev Cancer 1872(2):188308
111. Wang G, Mitomo H, Matsuo Y, Shimamoto N, Niikura K, Ijiro K (2013) DNA-templated plasmonic Ag/AgCl nanostructures for molecular selective photocatalysis and photocatalytic inactivation of cancer cells. J Mater Chem B 1(43):5899–5907
112. Seo JH, Jeon WI, Dembereldorj U, Lee SY, Joo S-W (2011) Cytotoxicity of serum protein-adsorbed visible-light photocatalytic Ag/AgBr/TiO_2 nanoparticles. J Hazard Mater 198:347–355

113. Kösters JP, Gøtzsche PC (2003) Regular self-examination or clinical examination for early detection of breast cancer. Cochrane Database Syst Rev (2)
114. King A, Woo J, Ai Q, Chan J, Lam W, Tse I et al (2019) Complementary roles of MRI and endoscopic examination in the early detection of nasopharyngeal carcinoma. Ann Oncol 30(6):977–982
115. Wang GL, Xu XF, Qiu L, Dong YM, Li ZJ, Zhang C (2014) Dual responsive enzyme mimicking activity of AgX (X=Cl, Br, I) nanoparticles and its application for cancer cell detection. ACS Appl Mater Interfaces 6(9):6434–6442
116. Song Y, Qu K, Zhao C, Ren J, Qu X (2010) Graphene oxide: intrinsic peroxidase catalytic activity and its application to glucose detection. Adv Mater 22(19):2206–2210
117. Tao Y, Lin Y, Huang Z, Ren J, Qu X (2013) Incorporating graphene oxide and gold nanoclusters: a synergistic catalyst with surprisingly high peroxidase-like activity over a broad pH range and its application for cancer cell detection. Adv Mater 25(18):2594–2599
118. Bharali DJ, Lucey DW, Jayakumar H, Pudavar HE, Prasad PN (2005) Folate-receptor-mediated delivery of InP quantum dots for bioimaging using confocal and two-photon microscopy. J Am Chem Soc 127(32):11364–11371
119. Song Y, Shi W, Chen W, Li X, Ma H (2012) Fluorescent carbon nanodots conjugated with folic acid for distinguishing folate-receptor-positive cancer cells from normal cells. J Mater Chem 22(25):12568–12573
120. Zhang B, Wang X, Zhao Y, Lv J, Meng H, Chang H et al (2017) Highly photosensitive colorimetric immunoassay for tumor marker detection based on Cu^{2+} doped Ag–AgI nanocomposite. Talanta 167:111–117
121. Mazhabi RM, Ge L, Jiang H, Wang X (2018) A label-free aptamer-based cytosensor for specific cervical cancer HeLa cell recognition through a gC_3N_4–AgI/ITO photoelectrode. J Mater Chem B 6(31):5039–5049
122. Cui D, Shi Y, Xing D, Yang S (2021) Ultrahigh sensitive and tumor-specific photoacoustography in NIR-II region: optical writing and redox-responsive graphic fixing by AgBr@ PLGA nanocrystals. Nano Lett 21(16):6914–6922
123. Mantri Y, Davidi B, Lemaster JE, Hariri A, Jokerst JV (2020) Iodide-doped precious metal nanoparticles: measuring oxidative stress in vivo via photoacoustic imaging. Nanoscale 12(19):10511–10520
124. Li P, Poon YF, Li W, Zhu H-Y, Yeap SH, Cao Y et al (2011) A polycationic antimicrobial and biocompatible hydrogel with microbe membrane suctioning ability. Nat Mater 10(2):149–156
125. Zhang L-j, Guerrero-Juarez CF, Hata T, Bapat SP, Ramos R, Plikus MV et al (2015) Dermal adipocytes protect against invasive Staphylococcus aureus skin infection. Science 347(6217):67–71
126. Zhou S, Li J, Gilroy KD, Tao J, Zhu C, Yang X et al (2016) Facile synthesis of silver nanocubes with sharp corners and edges in an aqueous solution. ACS Nano 10(11):9861–9870
127. Shah ZH, Wang J, Ge Y, Wang C, Mao W, Zhang S et al (2015) Highly enhanced plasmonic photocatalytic activity of Ag/AgCl/TiO_2 by CuO co-catalyst. J Mater Chem A 3(7):3568–3575
128. Zhu M, Chen P, Liu M (2011) Graphene oxide enwrapped Ag/AgX (X= Br, Cl) nanocomposite as a highly efficient visible-light plasmonic photocatalyst. ACS Nano 5(6):4529–4536
129. Yang Y, Zhang W, Liu R, Cui J, Deng C (2018) Preparation and photocatalytic properties of visible light driven Ag-AgBr-RGO composite. Sep Purif Technol 190:278–287
130. Zhang J, Wang J, Xu H, Lv X, Zeng Y, Duan J et al (2019) The effective photocatalysis and antibacterial properties of AgBr/$AgVO_3$ composites under visible-light. RSC Adv 9(63):37109–37118
131. Lin L, Xie Q, Zhang M, Liu C, Zhang Y, Wang G et al (2020) Construction of Z-scheme Ag–AgBr/$BiVO_4$/graphene aerogel with enhanced photocatalytic degradation and antibacterial activities. Colloids Surf A 601:124978
132. Li Z, Fu Y, Fang W, Li Y (2015) Electrochemical impedance immunosensor based on self-assembled monolayers for rapid detection of *Escherichia coli* O157:H7 with signal amplification using lectin. Sensors 15(8):19212–19224
133. Joung CK, Kim HN, Lim MC, Jeon TJ, Kim HY, Kim YR (2013) A nanoporous membrane-based impedimetric immunosensor for label-free detection of pathogenic bacteria in whole milk. Biosens Bioelectron 44:210–215
134. Tan F, Leung PHM, Liu ZB, Zhang Y, Xiao L, Ye W et al (2011) A PDMS microfluidic impedance immunosensor for *E. coli* O157:H7 and *Staphylococcus aureus* detection via antibody-immobilized nanoporous membrane. Sens Actuators B Chem 159(1):328–335
135. Varshney M, Li Y, Srinivasan B, Tung S (2007) A label-free, microfluidics and interdigitated array microelectrode-based impedance biosensor in combination with nanoparticles immunoseparation for detection of *Escherichia coli* O157:H7 in food samples. Sens Actuators B Chem 128(1):99–107
136. Wu S, Zhang J, Wu P (2019) Photo-modulated nanozymes for biosensing and biomedical applications. Anal Methods 11(40):5081–5088
137. Liu Y, Wang X, Wei H (2020) Light-responsive nanozymes for biosensing. Analyst 145(13):4388–4397
138. Hashemi SA, Mousavi SM, Bahrani S, Ramakrishna S (2020) Polythiophene silver bromide nanostructure as ultra-sensitive non-enzymatic electrochemical glucose biosensor. Eur Polym J 138:109959
139. Chen F, Liang W, Qin X, Jiang L, Zhang Y, Fang S et al (2021) Ag@AgCl photocatalyst loaded on the 3D graphene/PANI hydrogel for the enhanced adsorption-photocatalytic degradation and in situ SERS monitoring properties. ChemistrySelect 6(17):4166–4177
140. Zhu JH, Feng YG, Wang AJ, Mei LP, Luo X, Feng JJ (2021) A signal-on photoelectrochemical aptasensor for chloramphenicol assay based on 3D self-supporting AgI/Ag/BiOI Z-scheme heterojunction arrays. Biosens Bioelectron 181:113158
141. Zhang L, Shen YL, Fan GC, Xiong M, Yu XD, Zhao WW (2019) Preparation of an AgI/$CuBi_2O_4$ heterojunction on a fluorine-doped tin oxide electrode for cathodic photoelectrochemical assays: application to the detection of L-cysteine. Mikrochim Acta 186(5):284
142. Yan W, Feng X, Chen X, Hou W, Zhu JJ (2008) A super highly sensitive glucose biosensor based on Au nanoparticles-AgCl@polyaniline hybrid material. Biosens Bioelectron 23(7):925–931
143. Wu J, Wang X, Wang Q, Lou Z, Li S, Zhu Y et al (2019) Nanomaterials with enzyme-like characteristics (nanozymes): next-generation artificial enzymes (II). Chem Soc Rev 48(4):1004–1076
144. Li Y, Liu J (2021) Nanozyme's catching up: activity, specificity, reaction conditions and reaction types. Mater Horiz 8(2):336–350
145. Zandieh M, Liu J (2021) Nanozyme catalytic turnover and self-limited reactions. ACS Nano 15(10):15645–15655
146. Ozdemir C, Yeni F, Odaci D, Timur S (2010) Electrochemical glucose biosensing by pyranose oxidase immobilized in gold nanoparticle-polyaniline/AgCl/gelatin nanocomposite matrix. Food Chem 119(1):380–385
147. Hao N, Zhang X, Zhou Z, Hua R, Zhang Y, Liu Q et al (2017) AgBr nanoparticles/3D nitrogen-doped graphene hydrogel for fabricating all-solid-state luminol-electrochemiluminescence *Escherichia coli* aptasensors. Biosens Bioelectron 97:377–383

Publisher's Note